AN ANALYTICAL METHOD FOR INVESTIGATING TRANSIENT POTENTIALS IN NEURONS WITH BRANCHING DENDRITIC TREES

BARRY HORWITZ, *Department of Mathematics and Physics, Texas Woman's University, Denton, Texas 76204*

ABSTRACT An analytical method is developed that allows one to explore the way in which the geometrical structure of a neuron's dendritic tree affects the time-course and amplitude of transient potentials generated at different locations on dendritic branches. The method requires that, for a given dendritic arborization, one associates a symmetric geometry for which exact mathematical expressions for time-varying dendritic potentials can be calculated. The value of the dendritic potential for the asymmetric geometry is evaluated by adding correction terms to the results for the symmetric geometry. Several model trees are examined, and in each case the analytical results are expressed in terms of two closely related families of functions. These functions provide a precise formalism for systematically analyzing the way in which the voltage transient at a given point depends upon the geometrical structure of the dentritic tree. Several numerical examples are presented. A discussion of how to generalize the method and of some potential applications are given.

INTRODUCTION

In spite of many years of extensive research the neuron remains enigmatic. Although neuronal structure and function are inextricably intertwined, their relationship (with a few special exceptions) is essentially unknown to us. The awesome complexity of the dendritic tree makes it difficult to elucidate the neuron's passive integrative behavior, and prevents the dendritic tree's own functional role from being fully understood. In addition, until recently many crucial aspects of neuronal structure and function were beyond the resolving power of experimental analysis. In the last few years there have been a number of related developments that, when taken together, have allowed a finer assesssment of the dendritic structure-function relationship and a deeper appreciation of its significance for brain functioning.

The first of these has involved improvements in our ability to visualize neuronal structure. Dyes, which spread to all of a neuron's processes, can be injected electrophoretically into an identified cell body through the same micropipette used to detect the neuron's electrical activity. For example, the flourescent dyes Procion yellow and Lucifer yellow have been used extensively at the light microscopic level (some representative studies are Stretton and Kravitz, 1968; Van Essen and Kelly, 1973; Gutnick and Prince, 1981), while the enzyme horseradish peroxidase has been used both for light microscopic studies (e.g., Gilbert and Wiesel, 1979) and for those at the electron microscopic level (e.g., Christensen and Ebner, 1978). Along with comparable developments in the use of computer-assisted reconstruction techniques (see Lindsay, 1977, for a review), these advances make it now possible to visualize the complete three-dimensional morphology of a nerve cell whose electrophysiological

behavior has been recorded, and when applied to electron microscopic studies, to locate all the synapses impinging upon the reconstructed neuron. For example, Davis and Sterling (1979) reported that by reconstructing 32 adjacent neurons from electron micrographs of 150 serial sections through area 17 of the visual cortex, cells could be divided into seven classes based on differences not only in size, shape, and dendritic branching, but also on differences in synaptic input (the lateral geniculate nucleus had been destroyed before examination of the cortex). They concluded that lateral geniculate input is distributed in specific patterns in at least six of the seven classes of cortical cells they identified.

A second set of developments has arisen from the recent importance attached to local circuit neurons in our understanding of brain functioning. Evidence has accumulated that a majority of the neurons in the mammalian central nervous system possess relatively short processes and make contact only with neighboring neurons (Rakic, 1976; Schmitt et al., 1976; and Schmitt and Worden, 1979 provide useful reviews of this evidence, as well as overviews of this entire area). In contrast to long axon or projection neurons with integrative capabilities focused at the axon hillock, local circuit neurons mediate their interactions by graded electrotonic potentials and often interact with one another through high sensitivity (submillivolt threshold) dendrodendritic synapses.

The olfactory bulb provides a striking illustration of information processing in local neuronal circuits (Shepherd [1979, Chapter 8] provides an excellent discussion of this system). The afferent inputs to the bulb from receptor cells in the nasal cavity synapse onto mitral cell dendrities in spherical regions of neuropil called glomeruli (see Fig. 8.2 of Shepherd, 1979) where dendritic branches of one of the interneurons, the periglomerular cell, can also be found. The mitral cell, which has several secondary dendrites that make contact with another interneuron, the granule cell, finally gives rise to a long axon which becomes part of the lateral olfactory tract.[1] The mitral cell makes dendrodendritic synapses with both the granule cell (Rall et al., 1966) and the periglomerular cell (Pinching and Powell, 1971; White, 1972), and thus has both synaptic inputs and outputs from all parts of its dendritic tree. Electronic spread, apparently, is sufficient for conveying input electrical activity to the output regions in both the glomerulus and in the secondary dendritic regions; active spikes have been unequivocally identified only along the mitral cell's axon (Shepherd, 1979).

Finally, a large number of reports in the last few years have implicated changes in dendritic morphology with learning, aging, and certain mental diseases. Greenough and his collaborators, for example, have shown that the social and physical stimulation provided by an animal's rearing environment affects the branching of dendrites in several brain regions (e.g., Fiala et al., 1978; Greenough and Volkmar, 1973), and that dendritic modifications occur in adult rats following a specific learning experience (Greenough et al., 1979). Mehraein et al. (1975) reported that the extent of the dendritic tree, as well as the density of dendritic spines of pyramidal cells from the cingulate gyrus and the hippocampus were greatly reduced in patients with either senile dementia or Alzheimer's disease, while Purpura (1974) showed dendritic spine dysgenesis in cortical neurons in children with profound mental retardation. More recently, Buell and Coleman (1979) have presented evidence suggesting that the

[1] In this discussion we ignore other synaptic relationships, and other cells in the olfactory bulb as well.

dendritic tree of some cells continues to grow in normal human aging, while in senile dementia there is a failure of this sustained growth.

From the above developments we can infer that in the not-too-distant future experimental information will be available on the three-dimensional shape of neurons whose electrical activity has been monitored and on the location upon such a neuron of most or all of its synaptic inputs (many of whose regions of origin will be known). Coupling this with the research being done on local circuit neurons, particularly their way of transmitting and processing information electrotonically, and with the manifest importance between dendritic morphology and brain functioning, we see that it will be important to have available a neuronal model that treats the cable properties of the dendritic tree along with its complex geometry in a realistic fashion. Specifically, we would like to have a precise language (preferably mathematical) that can relate dendritic morphology to the spread of postsynaptic potentials.

Although neuronal models for studying the cable properties of dendritic trees have existed for a number of years, most have not considered how geometry affects a neuron's input-output characteristics. Instead, they have dealt with dendritic branches by lumping them together to avoid having to treat them individually. This is especially true for transient potentials. The best known and most fruitful of these models comes from the work at Wilfrid Rall (1959–1977). One of his most important discoveries was the equivalent cylinder class of dendritic trees (Rall, 1962*a*), for which it is possible to treat the entire tree mathematically as if it were a single cable. This way of modeling the passive behavior of a neuron has been used extensively by Rall (1962*a, b,* 1964, 1967, 1969) and others (e.g., Jack and Redman, 1971*a, b;* Redman, 1973). The equivalent cylinder class of Rall (see Fig. 1) is characterized by the 3/2-power law:

$$d_j^{3/2} = \sum_{k=1}^{N} d_{jk}^{3/2} \tag{1}$$

d_j is the diameter of the jth dendritic branch; d_{jk} are the diameters of the daughter branches into which it divides. It should be noted that Rall never proposed this as a law of nature. Although some observations (Lux et al., 1970) seemed to confirm the validity of the

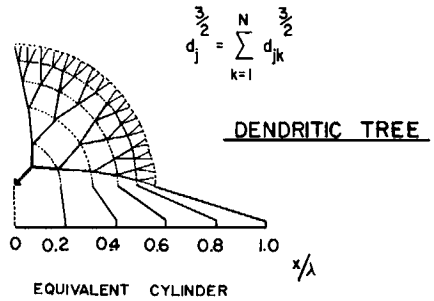

FIGURE 1 Diagram illustrating Rall's equivalent cylinder model. The symmetric dendritic tree will behave electrically the same as the equivalent cylinder if the 3/2 rule for branch diameters is obeyed. (Modified from Rall, 1962b)

relationship for motorneurons, other studies (Barrett and Crill, 1974*a*; Hillman, 1979) have reported substantial deviations from the 3/2 rule.

The specific assumptions associated with the use of the equivalent cylinder class of dendritic trees are the following:

(*a*) The 3/2 rule for dendritic diameters holds at each junction.

(*b*) Although branch lengths can be unequal, all terminal branches must end with the same boundary condition, and at the same electrotonic distance.

(*c*) Synaptic inputs are at the same electrotonic distance on all (Rall, 1962*a*, *b*, 1969; Jack and Redman, 1971*a*, *b*) or some (Redman, 1973) of the dendritic branches.

More recently, Rall and Rinzel have developed a formulation that relaxes this last assumption. They treat the situation where there is an input at only a single branch of a dendritic tree. Both steady-state (Rall and Rinzel, 1973) and transient potentials (Rinzel and Rall, 1974) are obtained.

The Rall model has contributed greatly to our understanding of neuronal behavior, especially on the dominance of the dendrites in determining the passive cable properties of the motorneuron, as measured at the soma (Rall, 1977; Redman, 1976). And indeed, one can argue that the assumptions made by Rall, Redman, and their collaborators to simplify the complexity of a dendritic system were crucial to the analysis, most particularly because of the limited experimental data available on the anatomical parameters of dendrites, on the electrophysiological parameters of dendrites, and on the location of synapses upon the dendrites. The theoretical work of Rall, Redman et al. has, in fact, been instrumental in enabling the values of some of these parameters to be determined (see Redman, 1976, for a review).

Nevertheless, because of the changing experimental scene discussed previously, certain simplifications in the Rall model can now be viewed as limiting the kinds of analyses that can be done. The major disadvantage of restricting one's attention to the equivalent cylinder class is that it eliminates the ability to assess how various portions of the dendritic tree "interact" with one another in determining the integrative properties of the neuron. Moreover, the local circuit features of a tree require a more realistic modeling of the geometry of a dendritic system, especially if one is investigating regional computation within a dendritic tree. Finally, there is little evidence in favor of the three assumptions listed above that are associated with the equivalent cylinder class. Redman's (1976) overview of the experimental situation leads him to conclude that even in motorneurons the validity of the 3/2 rule is questionable. The assumption that all branches of a dendritic tree are the same electrotonic length has also been questioned recently; Christensen and Teubl (1979) have presented some results that are incompatible with its validity. Hence, in order to extend the Rall model so that a greater understanding of the role played by the dendritic geometry can be acquired, it is necessary to study neurons that are not of the equivalent cylinder class. That is, a model should be developed that does not make use of the three assumptions listed above.

One way to do this, of course, is to employ the numerical modeling techniques of a compartmental analysis (Rall, 1964). In this approach one approximates a continuous dendrite (or dendritic tree) as a set of resistively coupled isopotential regions. Treatments of this kind have been performed on fairly complicated dendritic systems (e.g., Perkel and Mulloney, 1978; Glasser, 1977). However, while numerical methods are valuable for

examining a particular system, analytical expressions might permit one to find general properties of dendritic organization, thus enabling one to elucidate the significance of differing geometrical patterns of dendritic branching.

I have developed a theoretical method for determining analytical expressions for the time-course and amplitude of transient potentials in dendritic systems with fairly complicated geometries. The method provides a way to assess how the geometrical structure of a neuron's dendritic tree influences the propagation of postsynaptic potentials. My model is based upon the work of Butz and Cowan (1974), and it allows one to investigate neurons which are not of the equivalent cylinder class. Butz and Cowan developed a graphical calculus that generates analytic solutions for the Laplace transform of the membrane potential at any point on the dendritic tree of neurons with arbitrary dendritic geometries. My work provides a method for determining the inverse transform (which is the transmembrane potential change) in analytic form. Most significantly, all the results I have obtained are expressed in terms of two closely related families of functions, thus furnishing a suitable mathematical language with which to examine the dendritic structure-function relation.

BUTZ-COWAN MODEL

The Butz-Cowan (1974) model starts with the cable equation representation of electrotonic potentials in which a distributed model is used. First proposed by Rall two decades ago (Rall, 1959), the major assumptions made are the following (see Fig. 2): (*a*) all dendritic branches are treated as cylinders of uniform passive nerve membrane. A unit membrane area is represented as a capacitance in parallel with a voltage-independent (passive) resistance. (*b*) The extracellular space is assumed to be an isopotential. (*c*) Each unit of membrane is connected to its neighbors by core resistances, resulting in each cylinder being regarded as a one-dimensional cable of finite length. (*d*) At all branch points membrane potential is assumed to be continuous, and core current is conserved. These assumptions allow one to say that $v(x, t)$, the electric potential of the inside of a dendrite with respect to the outside, must be a solution of the cable differential equation (for a derivation of this result, see Jack et al.,

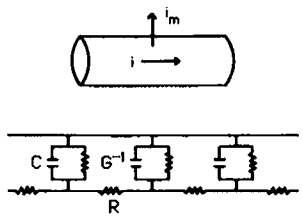

FIGURE 2

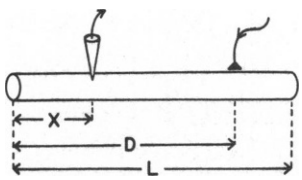

FIGURE 3

FIGURE 2 Cable model in one dimension. The upper diagram shows a dendritic branch with core current i and membrane current i_m. The lower diagram shows the equivalent electrical circuit: a unit area of membrane is represented by a capacitance (C) in parallel with a conductance (G); each unit area is linked to its neighbors by a core resistance (R).

FIGURE 3 Unbranched dendritic tree of length L with a recording electrode at x and a current input at a distance D from the origin.

1975):

$$\lambda^2 \frac{\partial^2 v(x, t)}{\partial x^2} - \tau \frac{\partial v(x, t)}{\partial t} - v(x, t) = 0 \tag{2}$$

x is the position along the dendrite, t is the time;

$$\lambda^2 = 1/RG \tag{3}$$

$$\tau = C/G. \tag{4}$$

R, C, and G are, respectively, the core resistance, the membrane capacitance, and the membrane conductance of the cable representing the dendrite.[2] For a given dendrite these parameters are taken to be constant. λ is called the space constant, and τ is the time constant of the branch. The membrane potential, $v(x, t)$, is measured relative to the resting potential. The electric current within the core is given by

$$i(x, t) = -\frac{1}{R} \frac{\partial v(x, t)}{\partial x}. \tag{5}$$

A standard way to solve the partial differential equation given by Eq. 2 employs Laplace transformation techniques (Churchill, 1958). We define the Laplace transforms of $v(x, t)$ and $i(x, t)$ by the following equations:

$$V(x, s) = \int_0^\infty v(x, t) e^{-st} \, dt \equiv \mathcal{L}v(x, t) \tag{6}$$

$$I(x, s) = \int_0^\infty i(x, t) e^{-st} \, dt \equiv \mathcal{L}i(x, t). \tag{7}$$

Eqs. 2 and 5 are then replaced by ordinary differential equations for the Laplace transforms:

$$\frac{d^2 V(x, s)}{dx^2} - \gamma^2 V(x, s) = 0 \tag{8}$$

$$\frac{dV(x, s)}{dx} + RI(x, s) = 0 \tag{9}$$

with

$$\gamma = \frac{\sqrt{s\tau + 1}}{\lambda}. \tag{10}$$

The general solution to these equations is easy enough to write down:

$$V(x, s) = A(s) \cosh \gamma x + B(s) \sinh \gamma x \tag{11}$$

[2]My notation follows that of Butz and Cowan (1974). In particular, the symbol L stands for the physical, rather than the electrotonic length of a branch.

and

$$I(x, s) = -\frac{1}{Z_c}[A(s) \sinh \gamma x + B(s) \cosh \gamma x] \tag{12}$$

where $Z_c = R/\gamma$ is called the characteristic impedance of the cable. The unknown constants $A(s)$ and $B(s)$, which are functions of the transform parameter s, are determined by the boundary conditions. For a branching dendritic tree the determination of A and B is very complicated.

Butz and Cowan (1974) developed a graphical calculus for generating analytical solutions for $V(x, s)$ at any point on the dendritic tree of neurons with arbitrary dendritic geometries. The $V(x, s)$ they calculate is in response to a synaptic current input at any specified point on the dendritic tree. Using their rules, one can write down the solution to Eq. 8 no matter how complicated the geometry. Essentially, they provide a systematic, nonrecursive way to determine $A(s)$ and $B(s)$ of Eq. 11. We shall illustrate their results with two examples. In both cases we take the ends of the dendritic branches to be "sealed" (i.e., open-circuit terminations).

Unbranched Dendritic Tree

Fig. 3 shows the geometry for this example, which is the simplest case: an unbranced tree of length L, a recording electrode at x (which is used symbolically to denote the point at which the potential is to be evaluated), and a synaptic input at D ($x < D$). Then,

$$V(x, s) = \frac{[\frac{x}{-}]^* [\frac{L - D}{-}]^*}{[\frac{L}{-}]} I_{sy}(s) \tag{13}$$

$$= \frac{Z_c \cosh \gamma x \cosh \gamma(L - D)}{\sinh \gamma L} I_{sy}(s) \tag{14}$$

where $I_{sy}(s) = \mathcal{L}\, i_{sy}(t)$, $i_{sy}(t)$ being the current produced by the synaptic input. Eq. 13 shows the diagramatic form for $V(x, s)$, whereas Eq. 14 gives the corresponding analytic expression.

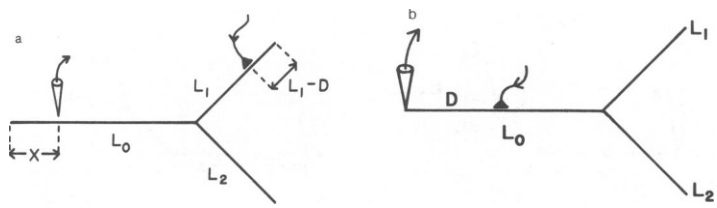

FIGURE 4 (*a*) A branched dendritic tree with one primary and two secondary branches. The current input is on a secondary branch, a distance D from the bifurcation. (*b*) A branched dendritic tree with one primary and two secondary branches. The current input is on the primary branch, a distance D from $x = 0$.

The translation between the two is given by

$$[\underline{\underline{x}}]^* = Z_c \cosh \gamma x \tag{15}$$

$$[\underline{\underline{L}}] = Z_c \sinh \gamma L. \tag{16}$$

One Bifurcation Point, One Proximal, Two Peripheral Branches

Fig. 4 *a* shows the geometry for this example, the second simplest case. The primary branch has length L_0, the secondary branches have lengths L_1 and L_2. There is a current source at some point D along the peripheral branch L_1. The rules of Butz and Cowan (1974) give us the following expression for the potential at a point x along the primary branch:

$$V(x, s) = \frac{Z_{c_0} Z_{c_1} Z_{c_2} [\underline{\underline{x}}]^* [\underline{\underline{L_2}}]^* [\underline{\underline{L_1 - D}}]^* I_{sy}(s)}{\left[\begin{array}{l} L_0 \quad L_1 \\ \qquad\quad L_2 \end{array}\right]^*} \tag{17}$$

$$= \frac{Z_{c_0} Z_{c_1} Z_{c_2} \cosh \gamma_0 x \cosh \gamma_2 L_2 \cosh \gamma_1 (L_1 - D)}{\left[\begin{array}{l} Z_{c_0} Z_{c_1} \cosh \gamma_0 L_0 \cosh \gamma_1 L_1 \sinh \gamma_2 L_2 \\ + Z_{c_0} Z_{c_2} \cosh \gamma_0 L_0 \sinh \gamma_1 L_1 \cosh \gamma_2 L_2 \\ + Z_{c_1} Z_{c_2} \sinh \gamma_0 L_0 \cosh \gamma_1 L_1 \cosh \gamma_2 L_2 \end{array}\right]} I_{sy}(s) \tag{18}$$

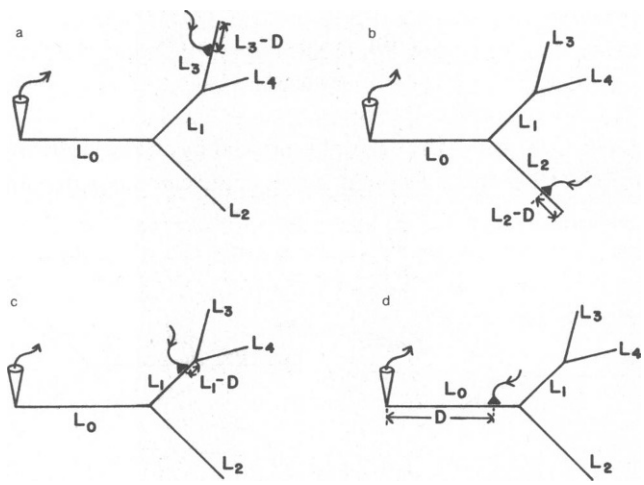

FIGURE 5 A branched dendritic tree with two bifurcations. (*a*) Current input on a tertiary branch, a distance D from the bifurcation; (*b*) current input on a terminal secondary branch; (*c*) current input on a nonterminal secondary branch; (*d*) current input on the primary branch.

where $Z_{c_i} = R_i/\gamma_i$ and $\gamma_i = (s\tau_i + 1)^{1/2}/\lambda_i$. Notice that the complexity of the mathematical expression for $V(x, s)$ increases dramatically as we increase the number of branches.

Figs. 5 and 6 show more complicated geometries. In these, and all other such cases, the rules of Butz and Cowan (1974) permit us to find $V(x, s)$. In addition, they provide rules that allow the boundary condition at the end of each dendritic branch to be independently specified. For example, one terminal may be represented by a sealed end boundary condition, whereas a second could have a "killed end" (closed circuit) terminal. Furthermore, their rules can incorporate the addition of a cell body at one terminal (e.g., $x = 0$). The cell body is best represented by a "lumped-soma" boundary condition (a conductance G_0 in parallel with a capacitance C_0). For a discussion of these boundary conditions, see Jack et al., 1975.

THE INVERSION OF $V(x, s)$

To utilize the Butz-Cowan formalism when dealing with transient potentials, we must find the inverse Laplace transform of $V(x, s)$:

$$v(x, t) = \mathcal{L}^{-1} V(x, s) \tag{19}$$

Butz and Cowan did not do this. However, $v(x, t)$ is the transmembrane potential difference, and so it is ultimately the quantity of both experimental and theoretical interest. Although numerical methods may be used, my objective is to generate analytical expressions for $v(x, t)$. Tables exist that provide the inverse Laplace transforms for a large number of common functions (Oberhettinger and Badii, 1973), but even a relatively simple branching system, such as in Fig. 4 *a*, produces a function, the $V(x, s)$ of Eq. 18, which is much too complicated to be found in these tables. Consequently, a different approach must be tried.

If one looks carefully at the equations of Butz and Cowan (1974), one finds that all of their results can be written in the following form:

$$V(x, s) = R(x, s) A(D, s) F(G, s) I_{sy}(s) \tag{20}$$

where $R(x, s)$ is a factor that depends upon the location at which the potential is to be evaluated (i.e., the recording electrode's position), $A(D, s)$ depends upon the position of the synaptic input, $F(G, s)$ depends upon the geometry of the dendritic tree, (the symbol G is used to denote this dependence) and $I_{sy}(s)$ is the Laplace transform of the input current. Of course, each of these is a function of the transform parameter, s. For example, for the tree shown in

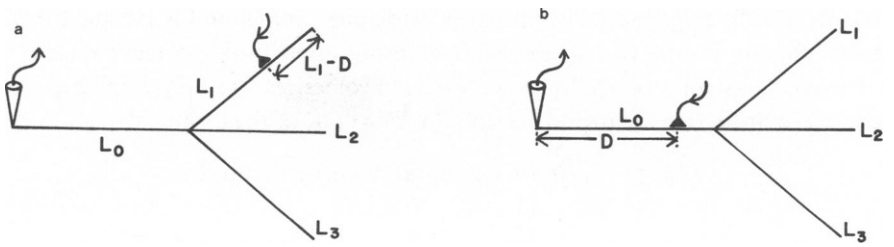

FIGURE 6 A branched dendritic tree with one primary and three secondary branches. (*a*) Current input on a secondary branch; (*b*) current input on the primary branch.

Fig. 4 *a* with $V(x, s)$ given by Eq. 18,[3]

$$R(x, s) = Z_{c_0} \cosh \gamma_0 x \tag{21}$$

$$A(D, s) = \frac{\cosh \gamma_1 (L_1 - D)}{\cosh \gamma_1 L_1} \tag{22}$$

$$F(G, s) = \frac{Z_{c_1} Z_{c_2} \cosh \gamma_1 L_1 \cosh \gamma_2 L_2}{\left[\begin{array}{l} Z_{c_0} Z_{c_1} \cosh \gamma_0 L_0 \cosh \gamma_1 L_1 \sinh \gamma_2 L_2 \\ + Z_{c_0} Z_{c_2} \cosh \gamma_0 L_0 \sinh \gamma_1 L_1 \cosh \gamma_2 L_2 \\ + Z_{c_1} Z_{c_2} \sinh \gamma_0 L_0 \cosh \gamma_1 L_1 \cosh \gamma_2 L_2 \end{array}\right]}. \tag{23}$$

Suppose we define the following inverse Laplace transforms:

$$r(x, t) = \mathcal{L}^{-1} R(x, s) \tag{24}$$

$$a(D, t) = \mathcal{L}^{-1} A(D, s) \tag{25}$$

$$f(G, t) = \mathcal{L}^{-1} F(G, s), \tag{26}$$

then the convolution theorem (Churchill, 1958) may be used to obtain an expression for $v(x, t)$:

$$v(x, t) = \int_0^t dt_2 \int_0^{t_2} dt_3 \int_0^{t_3} dt_4\, r(x, t_4) f(G, t_3 - t_4) a(D, t_2 - t_3) i_{sy}(t - t_2). \tag{27}$$

This form for $v(x, t)$ offers more hope for evaluating the dendritic contribution to the way synaptic inputs affect the cell body. The crucial aspects can be summarized as follows:

(*a*) The Laplace transform of the dendritic potential, $V(x, s)$, is in a mathematical form whereby the geometry of the dendritic tree, the recording electrode's position, and the synapse's position occur in separate factors.

(*b*) By using the convolution theorem we have preserved, in a sense, this separation of factors in the mathematical expression for $v(x, t)$.

(*c*) Consequently, since each factor has been separated out, approximations can be applied to each without changing the others. In particular, we may study Eq. 26 to see how significant the various parts of a dendritic tree are to $v(x, t)$.

As can be seen from Eq. 27, after $r(x, t)$, $f(G, t)$ and $a(D, t)$ are found, $v(x, t)$ is obtained by evaluating an integral involving each of the separate inverse transforms. Generally, it is not possible to find exact mathematical expressions for the inverse transforms. However, if the dendritic arborization possesses certain symmetries, one can obtain the inverse transforms of the various factors in analytical form without using approximation techniques. I call the integral expressions for $v(x, t)$ for these special geometries "primitive integrals." For an asymmetric dendritic tree the expression for $v(x, t)$ will be of the form:

$$v(x, t) = \text{primitive integral} + \text{correction terms}. \tag{28}$$

[3]The choice of which terms to include in R, F, and A is not obvious. The forms given by Eqs. 21–23 represent the most appropriate choice. The rationale used is explained in the Discussion section of this paper. There, we shall also see that $A(D, s)$ is not totally independent of the geometry.

Although highly idealized, the geometries corresponding to the primitive integrals provide ample diversity to investigate the structure-function relationship. The correction terms can be evaluated by means of standard approximation techniques, such as the use of a Taylor series. Most of the remainder of this paper will be concerned with the primitive integrals, although one example will illustrate the asymmetric situation; future papers will address the asymmetric cases in a more detailed fashion.

THE PRIMITIVE INTEGRALS

The above method was used to study a number of dendritic geometries. Essentially, we began with the simpler cases and progressed to more complicated ones. In each we have obtained the primitive integrals in analytical form for all possible positions of the synaptic input. In all the cases we have assumed sealed end boundary conditions for each branch termination. In addition, for every configuration we have taken the recording position to be $x = 0$, which means that $r(x, t)$, the inverse transform of the factor involving the recording electrode's position, is the same for each case; it is the factors $a(D, t)$ and $f(G, t)$ that vary. We also assume the time constant (τ) is constant everywhere in the dendritic tree. A crucial assumption made for deriving the primitive integrals is that each branch has the same diameter. This implies essentially that the space constant (λ) and the characteristic impedance (Z_c) are constant throughout the tree. Approximations must be used when branch diameters are not uniform. Therefore, most of our illustrations will focus entirely on branch length and branch number as the geometrical parameters of interest.

The primitive integrals correspond to dendritic arborizations which possess certain symmetries: (*a*) a tree in which the lengths of all the branches are integral multiples of some fundamental length; or, (*b*) a tree in which one or more branches are taken to be infinitely long, and the lengths of remaining branches are integral multiples of some fundamental length. The latter geometries approximate the situation where some branches are very long relative to others.

The remarkable outcome of this analysis is that the results can be expressed in terms of two closely related families of functions, which we call the *G*-functions. They are defined as follows:

$$G_{mn;c}(L - D, t) = \mathcal{L}^{-1}\left\{\frac{\cosh \gamma(L - D)}{m \sinh \gamma L + n \cosh \gamma L}\right\} \tag{29}$$

$$G_{mn;s}(L - D, t) = \mathcal{L}^{-1}\left\{\frac{\sinh \gamma(L - D)}{m \sinh \gamma L + n \cosh \gamma L}\right\}. \tag{30}$$

The inverse transforms of the expressions within the brackets can be determined by writing the hyperbolic functions as exponentials. To illustrate,

$$\frac{\cosh \gamma(L - D)}{m \sinh \gamma L + n \cosh \gamma L} = \frac{e^{-\gamma D}[1 + e^{-2\gamma(L-D)}]}{(m + n)\left[1 - \left(\frac{m - n}{m + n}\right)e^{-2\gamma L}\right]}$$

$$= \frac{1}{m + n}\sum_{k=0}^{\infty}\left(\frac{m - n}{m + n}\right)^k \{e^{-\gamma(2kL + D)} + e^{-\gamma[2(k+1)L - D]}\}. \tag{31}$$

Defining[4]

$$g(x, t) = \sqrt{\frac{\tau}{\pi}} \frac{x}{2\lambda t^{3/2}} e^{-t/\tau} e^{-\tau x^2/4\lambda^2 t} \tag{32}$$

and using $\mathcal{L}^{-1} \exp(-\gamma x) = g(x, t)$ (Oberhettinger and Badii, 1973), we get

$$G_{mn;c}(L - D, t) = \frac{1}{m + n} \sum_{k=0}^{\infty} \left(\frac{m - n}{m + n}\right)^k \{g[2kL + D, t] + g[2(k + 1)L - D, t]\}. \tag{33}$$

Similarly,

$$G_{mn;s}(L - D, t) = \frac{1}{m + n} \sum_{k=0}^{\infty} \left(\frac{m - n}{m + n}\right)^k \{g[2kL + D, t] - g[2(k + 1)L - D, t]\}. \tag{34}$$

The infinite series that define the G-functions converge absolutely. The time behavior of these functions is illustrated in Figs. 7 and 8.

All the results I have obtained involve different combinations of these G-functions. The Gs that enter differ from one another primarily in the values of m and n; that is, in the values of the coefficients of each term of the series. To see the elegance and simplicity of this formalism we turn to the specific cases studied.

SPECIFIC APPLICATIONS

Unbranched Tree

(See Fig. 3 for the configuration.) From Eq. 14

$$V(0, s) = \frac{Z_c \cosh \gamma(L - D)}{\sinh \gamma L} I_{sy}(s). \tag{35}$$

Choosing

$$R(0, s) = Z_c = \frac{R}{\gamma} \tag{36}$$

$$A(D, s) = \frac{\cosh \gamma(L - D)}{\sinh \gamma L} \tag{37}$$

$$F(G, s) = 1 \tag{38}$$

gives us

$$r(0, t) = \frac{R\lambda}{\sqrt{\tau}} \frac{e^{-t/\tau}}{\sqrt{\pi t}} \tag{39}$$

---

[4]The function $g(x, t)$, except for the factor $\exp(-t/\tau)$, is essentially the so-called derived source solution of the diffusion equation. The unit source solution of the equation $u_{xx} - u_t = 0$ is given by $u_0(x, t) = \exp(x^2/4t)/\sqrt{4\pi t}$, and the derived source solution is defined as $h(x, t) = xu_0(x, t)/t$. We see that $g(x, t) = \tau^{-1}\exp(-t/\tau)\, h(x/\lambda, t/\tau)$. A good discussion of the mathematics of these solutions can be found in Widder (1975).

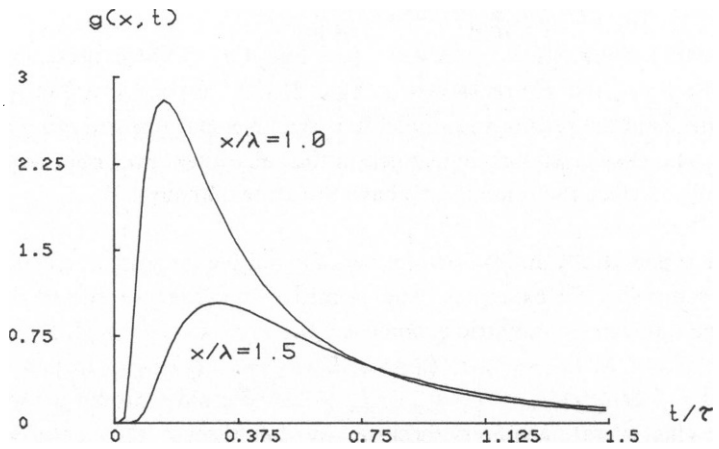

FIGURE 7 A plot of $g(x, t)$ vs. t for two values of the ratio x/λ. Notice that as x increases, the maximum value of g becomes smaller, and occurs later in time. The units were chosen so that $\tau = (2\sqrt{\pi})^{-1}$.

$$a(D, t) = G_{10;c}(L - D, t) \tag{40}$$

$$f(G, t) = \delta(t) \tag{41}$$

where $\delta(t)$ is the Dirac delta function.

It should be mentioned that Eq. 40 is not the standard way to write the inverse transform of the function given by the right-hand-side of Eq. 37. Generally, the inverse transforms of such functions are expressed in terms of theta and modified theta functions, and their derivatives (see Oberhettinger and Badii, 1973). The use of the G-function formalism offers a much clearer and more coherent way to write these inverses, as is demonstrated in Appendix B.

The expression for $v(x, t)$ is obtained by inserting Eqs. 39–41 into Eq. 27.

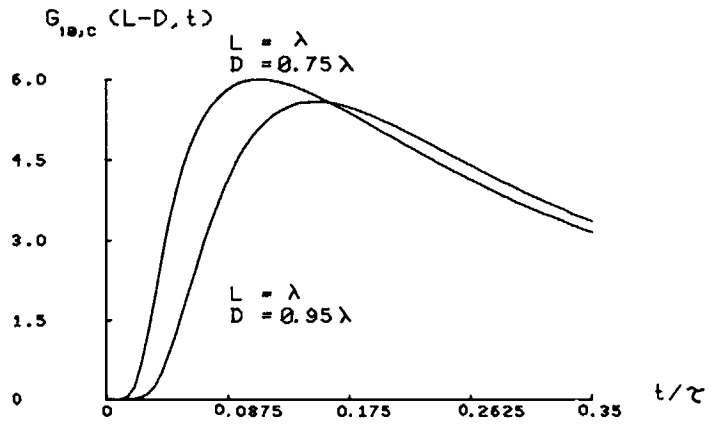

FIGURE 8 A plot of $G_{10;c}(L - D, t)$ vs. t. As D becomes larger, the maximum of $G_{10;c}$ becomes smaller, and occurs later in time. As in Fig. 7, the units are such that $\tau = (2\sqrt{\pi})^{-1}$.

One Main, Two Peripheral Branched Tree

A. INPUT ON PERIPHERAL BRANCH (see Fig. 4 *a*). The expression for $V(x, s)$ is given by Eq. 18; R, A and F are shown in Eqs. 21–23, respectively. Because $R(0, s)$ is precisely the same as in the previous example, so is the inverse transform $r(0, t)$, given by Eq. 39. Indeed, because $r(0, t)$ remains unchanged in the subsequent examples as well, it will no longer be mentioned. Since the branches all have the same diameter, $Z_{c_0} = Z_{c_1} = Z_{c_2}$ and $\gamma_0 = \gamma_1 = \gamma_2$.

Because there is potentially an infinite number of primitive integrals, we can only illustrate the results for some specific examples. The primitive integrals we choose as illustrations correspond to the following symmetric geometries: (*a*) $L_0 = L_1 = L_2 \equiv L$; (*b*) $L_0 = L_1 \equiv L$; $L_2 \rightarrow \infty$; (*c*) $L_0 = L_2 \equiv L$; $L_1 \rightarrow \infty$; (*d*) $L_0 \equiv L$; $L_1, L_2 \rightarrow \infty$; (*e*) $L_0 \equiv L$; $L_1 = L_2 = 2L$; (*f*) $L_0 = L_2 \equiv L$; $L_1 = 2L$; (*g*) $L_0 = L_1 = 2L$; $L_2 = 3L$. We have chosen a large number of illustrations for this overall geometry because we can discuss the analysis used with a minimum amount of algebraic complication.

(*a*) $L_0 = L_1 = L_2 \equiv L$ The expressions for $A(D, s)$ and $F(G, s)$ reduce to the following:

$$A(D, s) = \frac{\cosh \gamma(L - D)}{\cosh \gamma L} \tag{42}$$

$$F(G, s) = \frac{1}{3 \sinh \gamma L}. \tag{43}$$

We get

$$a(D, t) = G_{01;c}(L - D, t) \tag{44}$$

and

$$f(G, t) = \tfrac{1}{3} G_{10;c}(0, t). \tag{45}$$

(*b*) $L_0 = L_1 \equiv L$; $L_2 \rightarrow \infty$ The expressions for $A(D, s)$ and $a(D, t)$ remain unchanged. $F(G, s)$ reduces to

$$F(G, s) = \frac{1}{2 \sinh \gamma L + \cosh \gamma L} \tag{46}$$

which gives

$$f(G, t) = G_{21;c}(0, t) \tag{47}$$

(*c*) $L_0 = L_2 \equiv L$; $L_1 \rightarrow \infty$ The expressions for $F(G, s)$ and $f(G, t)$ are the same as in the previous case, i.e., Eqs. 46 and 47; $A(D, s)$ becomes

$$A(D, s) = e^{-\gamma D} \tag{48}$$

and thus,

$$a(D, t) = g(D, t). \tag{49}$$

(*d*) $L_0 \equiv L; L_1, L_2 \to \infty$ $A(D, s)$ and $a(D, t)$ are given by Eqs. 48 and 49, respectively; we also find

$$F(G, s) = \frac{1}{\sinh \gamma L + 2 \cosh \gamma L} \tag{50}$$

$$f(G, t) = G_{12;c}(0, t) \tag{51}$$

(*e*) $L_0 \equiv L; L_1 = L_2 = 2L$ For this case

$$A(D, s) = \frac{\cosh \gamma(L_1 - D)}{\cosh \gamma L_1} = \frac{\cosh \gamma(2L - D)}{\cosh 2\gamma L} \tag{52}$$

which yields

$$a(D, t) = G_{01;c}(2L - D, t). \tag{53}$$

The expression for $F(G, s)$ is

$$F(G, s) = \frac{\cosh^2 2\gamma L}{2 \cosh \gamma L \cosh 2\gamma L \sinh 2\gamma L + \sinh \gamma L \cosh^2 2\gamma L}$$

$$= \frac{1}{5 \sinh \gamma L} + \frac{2}{5}\left\{\frac{1}{\sinh \gamma L + i\sqrt{5} \cosh \gamma L} + \frac{1}{\sinh \gamma L - i\sqrt{5} \cosh \gamma L}\right\} \tag{54}$$

which gives

$$f(G, t) = \tfrac{1}{5} G_{10;c}(0, t) + \tfrac{2}{5}\{G_{1i\sqrt{5};c}(0, t) + G_{1-i\sqrt{5};c}(0, t)\}. \tag{55}$$

Although each of the two terms within the brackets in Eq. 55 contains both real and imaginary parts, the sum, and thus $f(G, t)$, is purely real.

(*f*) $L_0 = L_2 \equiv L; L_1 = 2L$ $A(D, s)$ and $a(D, t)$ remain unchanged from the previous case, and therefore are given by Eqs. 52 and 53, respectively. We find

$$F(G, s) = \frac{\cosh \gamma L \cosh 2\gamma L}{\cosh^2 \gamma L \sinh 2\gamma L + 2 \sinh \gamma L \cosh \gamma L \cosh 2\gamma L} \tag{56}$$

$$= \frac{1}{4 \sinh \gamma L} + \frac{1}{8}\left\{\frac{1}{\sinh \gamma L + i\sqrt{2} \cosh \gamma L} + \frac{1}{\sinh \gamma L - i\sqrt{2} \cosh \gamma L}\right\} \tag{57}$$

and thus,

$$f(G, t) = \tfrac{1}{4} G_{10;c}(0, t) + \tfrac{1}{8}\{G_{1i\sqrt{2};c}(0, t) + G_{1-i\sqrt{2};c}(0, t)\}. \tag{58}$$

As before, $f(G, t)$ is purely real.

(*g*) $L_0 = L_1 = 2L; L_2 = 3L$ Because this example is algebraically involved, we spell out some of the intermediate steps. As in (*e*) and (*f*), $a(D, t)$ is given by Eq. 53. The geometry-dependent factor is written

$$F(G, s) = \frac{\cosh 2\gamma L \cosh 3\gamma L}{\cosh^2 2\gamma L \sinh 3\gamma L + 2 \cosh 2\gamma L \sinh 2\gamma L \cosh 3\gamma L}. \tag{59}$$

This can be simplified by writing each hyperbolic factor in terms of sinh γL and cosh γL:

$$F(G, s) = \frac{4\cosh^3 \gamma L - 3\cosh \gamma L}{4\sinh \gamma L\,(\sinh^4 \gamma L + 4\cosh^4 \gamma L + \sinh^2 \gamma L \cosh^2 \gamma L + \tfrac{3}{4}\sinh^2 \gamma L - \tfrac{9}{4}\cosh^2 \gamma L)}$$

$$= (4\cosh^3 \gamma L - 3\cosh \gamma L)/[24(1-\alpha_1)(1-\alpha_2)\sinh \gamma L\,(\sinh \gamma L + i\beta_1 \cosh \gamma L)$$
$$\cdot\,(\sinh \gamma L - i\beta_2 \cosh \gamma L)(\sinh \gamma L + i\beta_2 \cosh \gamma L)(\sinh \gamma L - i\beta_2 \cosh \gamma L)] \quad (60)$$

where $\alpha_1 = 0.3104$, $\alpha_2 = 0.9395$, $\beta_1 = [\alpha_1/(1-\alpha_1)]^{1/2} = 0.6709$ and $\beta_2 = [\alpha_2/(1-\alpha_2)]^{1/2} = 3.9406$. Eq. 60 can be further simplified by use of the method of partial fractions:

$$F(G, s) = \left[\frac{0.1430}{\sinh \gamma L} + 0.0258\left(\frac{1}{\sinh \gamma L + \beta_1 \cosh \gamma L} + \frac{1}{\sinh \gamma L - i\beta_1 \cosh \gamma L}\right)\right.$$
$$\left. -0.0973\left(\frac{1}{\sinh \gamma L + i\beta_2 \cosh \gamma L} + \frac{1}{\sinh \gamma L - i\beta_2 \cosh \gamma L}\right)\right]\frac{1}{\cosh \gamma L} \quad (61)$$

and thus,

$$f(G, t) = \{0.1430\,G_{10;c}(0, t) + 0.0258[G_{1i\beta_1;c}(0, t) + G_{1-i\beta_1;c}(0, t)]$$
$$- 0.0973[G_{i\beta_2;c}(0, t) + G_{1-i\beta_2;c}(0, t)]\} * G_{01;c}(0, t). \quad (62)$$

The asterisk in Eq. 62 means convolution, i.e., $m(t)*n(t) = \int_0^t m(t')n(t-t')\mathrm{d}t'$. This example illustrates an important point: although the algebra can become tedious, this method of analysis can yield an exact result for $f(G, t)$ for any geometry in which the branch lengths are integral multiples of a fundamental length.

As can be seen from these results, the simplicity of the G-function notation is manifest. Notice, for example, how differences in the inverse transform of the geometry factor, $f(G, t)$, are reflected in the values assigned to the G-function indices. Note, as well, that $a(D, t)$, the inverse transform of the input factor, is written either as a G-function, when the branch upon which the synapse resides is of finite length, or more simply as $g(D, t)$ when the branch upon which the synapse is located is infinitely long.

Inserting the expressions for $f(G, t)$, $a(D, t)$ and $r(0, t)$ into Eq. 27 enables us to calculate the time-course and amplitude of the transient potential change at $x = 0$ in response to a current input at D on a peripheral branch. As an example, for the case where all three branches are of equal length we get

$$v(0, t) = \frac{R\lambda}{3\sqrt{\tau\pi}}\int_0^t \mathrm{d}t_2 \int_0^{t_2} \mathrm{d}t_3 \int_0^{t_3} \mathrm{d}t_4 \frac{e^{-t_4/\tau}}{\sqrt{t_4}}$$
$$\cdot\, G_{10;c}(0, t_3 - t_4)G_{01;c}(L - D, t_2 - t_3)i_{sy}(t - t_2). \quad (63)$$

We will discuss this expression in more detail in the section Numerical Example.

B. INPUT ON PROXIMAL BRANCH (See Fig. 4 *b*). The general expression for $V(x, s)$ is given by (Butz and Cowan, 1974)

$$V(x,s) = \frac{Z_{c_0}\cosh\gamma_0 x \begin{bmatrix} Z_{c_0}Z_{c_1}\sinh\gamma_0(L_0-D)\cosh\gamma_1 L_1\sinh\gamma_2 L_2 \\ +\, Z_{c_0}Z_{c_2}\sinh\gamma_0(L_0-D)\sinh\gamma_1 L_1\cosh\gamma_2 L_2 \\ +\, Z_{c_1}Z_{c_2}\cosh\gamma_0(L_0-D)\cosh\gamma_1 L_1\cosh\gamma_2 L_2 \end{bmatrix}}{\begin{bmatrix} Z_{c_0}Z_{c_1}\cosh\gamma_0 L_0\cosh\gamma_1 L_1\sinh\gamma_2 L_2 \\ +\, Z_{c_0}Z_{c_2}\cosh\gamma_0 L_0\sinh\gamma_1 L_1\cosh\gamma_2 L_2 \\ +\, Z_{c_1}Z_{c_2}\sinh\gamma_0 L_0\cosh\gamma_1 L_1\cosh\gamma_2 L_2 \end{bmatrix}} I_{sy}(s). \quad (64)$$

We choose

$$R(x,s) = Z_{c_0}\cosh\gamma_0 x \quad (65)$$

$$F(G,s) = 1 \quad (66)$$

$$A(D,s) = \frac{\Delta_N}{\Delta_1} \quad (67)$$

with

$$\Delta_N = \begin{matrix} Z_{c_0}Z_{c_1}\sinh\gamma_0(L_0-D)\cosh\gamma_1 L_1\sinh\gamma_2 L_2 \\ +\, Z_{c_0}Z_{c_2}\sinh\gamma_0(L_0-D)\sinh\gamma_1 L_1\cosh\gamma_2 L_2 \\ +\, Z_{c_1}Z_{c_2}\cosh\gamma_0(L_0-D)\cosh\gamma_1 L_1\cosh\gamma_2 L_2 \end{matrix} \quad (68)$$

$$\Delta_1 = \begin{matrix} Z_{c_0}Z_{c_1}\cosh\gamma_0 L_0\cosh\gamma_1 L_1\sinh\gamma_2 L_2 \\ +\, Z_{c_0}Z_{c_2}\cosh\gamma_0 L_0\sinh\gamma_1 L_1\cosh\gamma_2 L_2 \\ +\, Z_{c_1}Z_{c_2}\sinh\gamma_0 L_0\cosh\gamma_1 L_1\cosh\gamma_2 L_2. \end{matrix} \quad (69)$$

As before we take $x = 0$, $Z_{c_i} = Z_c$ and $\gamma_i = \gamma$ $(i = 0, 1, 2)$. Thus, $r(0, t)$ is given by Eq. 39. We calculate the primitive integrals for the same symmetric geometries as in the previous section, except we delete the last case ($L_0 = L_1 = 2L$, $L_2 = 3L$). For each geometry $f(G, t) = \delta(t)$.

(*a*) $L_0 = L_1 = L_2 \equiv L$ The expression for $A(D, s)$ reduces to

$$A(D,s) = \frac{2}{3}\frac{\sinh\gamma(L-D)}{\cosh\gamma L} + \frac{1}{3}\frac{\cosh\gamma(L-D)}{\sinh\gamma L} \quad (70)$$

which implies

$$a(D,t) = \tfrac{2}{3}\,G_{01;s}(L-D,t) + \tfrac{1}{3}\,G_{10;c}(L-D,t). \quad (71)$$

(*b*) $L_0 = L_1 = L$; $L_2 \to \infty$ *or* (*c*) $L_0 = L_2 = L$; $L_1 \to \infty$ These two geometries give identical results:

$$A(D,s) = \frac{\sinh\gamma(L-D)(1+\tanh\gamma L)}{2\sinh\gamma L + \cosh\gamma L} + \frac{\cosh\gamma(L-D)}{2\sinh\gamma L + \cosh\gamma L} \quad (72)$$

and

$$a(D,t) = \tfrac{1}{2}\,G_{21;s}(L-D,t) + \tfrac{1}{2}\,G_{01;s}(L-D,t) + G_{21;c}(L-D,t). \quad (73)$$

(*d*) $L_0 = L$; $L_1, L_2 \to \infty$ $A(D, s)$ takes the form

$$A(D, s) = \frac{2 \sinh \gamma(L - D) + \cosh \gamma(L - D)}{\sinh \gamma L + 2 \cosh \gamma L} \tag{74}$$

which yields

$$a(D, t) = 2\, G_{12;s}\,(L - D, t) + G_{12;c}\,(L - D, t). \tag{75}$$

(*e*) $L_0 = L$; $L_1 = L_2 = 2L$The algebra here is a bit involved; the procedure used to simplify the expression for $A(D, s)$ is similar to that delineated in (*g*) of the section: Input on Peripheral Branch. We find

$$A(D, s) = \frac{\cosh \gamma\,(L - D)}{5}\left(\frac{1}{\sinh \gamma L} + \frac{2}{\sinh \gamma L + i\sqrt{5} \cosh \gamma L} + \frac{2}{\sinh \gamma L - i\sqrt{5} \cosh \gamma L}\right)$$
$$+ \frac{2i}{\sqrt{5}} \sinh \gamma(L - D)\left(\frac{1}{\sinh \gamma L + i\sqrt{5} \cosh \gamma L} - \frac{1}{\sinh \gamma L - i\sqrt{5} \cosh \gamma L}\right) \tag{76}$$

$$a(D, t) = \tfrac{1}{5}[G_{10;c}(L - D, t) + 2G_{1i\sqrt{5};c}(L - D, t) + 2G_{1-i\sqrt{5};c}(L - D, t)]$$
$$+ \frac{2i}{\sqrt{5}}[G_{1i\sqrt{5};s}(L - D, t) - G_{1-i\sqrt{5};s}(L - D, t)]. \tag{77}$$

Note that the expression in the brackets in the second term of Eq. 77 is purely imaginary, and therefore the second term, and $a(D, t)$, are real.

(*f*) $L_0 = L_1 = L$; $L_2 = 2L$ *or* $L_0 = L_2 = L$; $L_1 = 2L$ Both of these geometries give identical, albeit lengthy, results:

$$A(D, s) = \frac{\sinh \gamma(L - D)}{4 \cosh \gamma L}\left\{\frac{\sinh \gamma L + \frac{3i}{\sqrt{2}} \cosh \gamma L}{\sinh \gamma L + i\sqrt{2} \cosh \gamma L} + \frac{\sinh \gamma L - \frac{3i}{\sqrt{2}} \cosh \gamma L}{\sinh \gamma L - i\sqrt{2} \cosh \gamma L}\right\}$$
$$+ \frac{\cosh \gamma(L - D)}{4 \sinh \gamma L}\left\{\frac{\sinh \gamma L + \frac{i}{\sqrt{2}} \cosh \gamma L}{\sinh \gamma L + i\sqrt{2} \cosh \gamma L} + \frac{\sinh \gamma L - \frac{i}{\sqrt{2}} \cosh \gamma L}{\sinh \gamma L - i\sqrt{2} \cosh \gamma L}\right\} \tag{78}$$

$$a(D, t) = \tfrac{1}{2}G_{01;s}(L - D, t) + \tfrac{1}{4}G_{10;c}(L - D, t)$$
$$+ \frac{i}{4\sqrt{2}}[G_{1i\sqrt{2};s}(L - D, t) - G_{1-i\sqrt{2};s}(L - D, t)]$$
$$+ \tfrac{1}{8}[G_{1i\sqrt{2};c}(L - D, t) + G_{1-i\sqrt{2};c}(L - D, t)]. \tag{79}$$

As in previous cases, $a(D, t)$ is a purely real function.

We note that the choice of expressions for $a(D, t)$ and $f(G, t)$ are different here than in the case where the synapse was located on a secondary branch. Rather than commenting on these differences now, we shall postpone giving the rationale behind the choices until the Discussion section. We shall then see that some general statements can be made about which expressions are most appropriate for a given geometry.

Other Geometries

Although the mathematics can become fairly involved, other, more complicated arborizations can be treated by this method. Exact expressions can be found for $a(D, t)$ and $f(G, t)$ for the symmetric geometries. These expressions always are written in terms of the G-functions. In Appendix A we present the results for some illustrative cases corresponding to dendritic trees with either two bifurcations (Fig. 5), or one primary and three secondary branches (Fig. 6).

NUMERICAL EXAMPLES

To illustrate the results obtained in the previous section, I shall compare the transient voltages for several of the above cases. This analysis will show that changes in the dendritic morphology can affect the way a postsynaptic potential (PSP) is perceived elsewhere in a dendritic tree. It should be emphasized that the numerical results presented below are meant to illuminate the kinds of behavior associated with the G-function formalism. A more detailed numerical study of the relationship between geometry and voltage will be presented elsewhere (Horwitz, 1981).

The first numerical example corresponds to the configurations shown in Fig. 4 *a*. I take each branch to be of length $L = \lambda$. Inserting the appropriate expressions for $r(0, t)$, $a(D, t)$ and $f(G, t)$ into Eq. 27 enables us to calculate the time-course and amplitude for the transient potential change at $x = 0$ in response to a current input at D on a peripheral branch.[5] Fig. 9 *a*

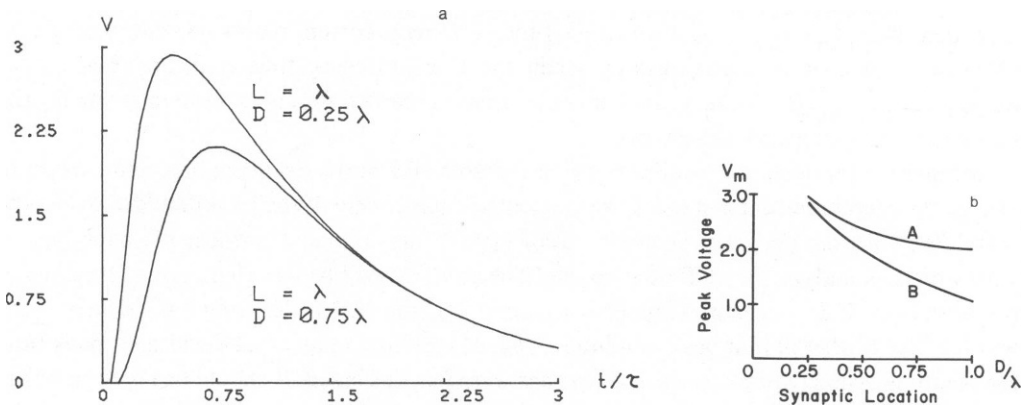

FIGURE 9 (*a*) A plot of $v(0, t)$ for the geometry of Fig. 4 *a* with the three branches of equal length. The diagram illustrates that the maximum of $v(0, t)$ is smaller, and occurs at a later time the further the current input is from $x = 0$. The units are such that $\tau = (2\sqrt{\pi})^{-1}$, $R\lambda = 3\sqrt{\pi}$, $Q = 1$. Each branch has length equal to the space constant. The input is located one-quarter length from the bifurcation in the top curve, and three-quarters length in the bottom curve. (*b*) A plot of the peak value of the voltage (v_m) vs. input location on the secondary branch (D). Curve *A* corresponds to the case where all three branches have equal length; for curve *B* the secondary branch on which the input is located is twice as long as the other two branches. The units are the same as above.

[5]The numerical integrations in this section were performed on a DEC-20 computer using a Romberg integration algorithm when the integrand consisted of a function; a cubic spline algorithm was employed when the integrand consisted of a list of values obtained by a prior integration. The algorithms can be found in Davis and Rabinowitz (1975); they are called CADRE and CUBINT, respectively.

shows the time behavior of $v(0, t)$ for two locations of the synaptic input; I have chosen $i_{sy}(t) = \delta(t)$, which corresponds to the injection of an instantaneous point charge of unit magnitude at $t = 0$. As expected, the peak value of the potential change at $x = 0$, denoted as v_m, decreases as the synaptic input is moved further away from the recording location. An explicit display of this is shown in Fig. 9 *b* (top curve). Changing the geometry can affect the peak voltage; the bottom curve of Fig. 9 *b* shows how the v_m vs. D behavior is changed when the branch upon which the synapse impinges doubles in length.

Another example is obtained by comparing geometries for which the synaptic location is the same, but in which we have different dendritic branchings. For this I shall use the unbranched geometry (Fig. 3) and the simple branching system shown in Fig. 4 *b*, in which the synapse is located on the primary branch. The expressions for $a(D, t)$ are given by Eqs. 40 and 71, respectively; $f(G, t) = \delta(t)$ for both cases. Fig. 10 displays a plot of the peak voltage, v_m, as a function of the D, the distance from the synaptic input to the recording point ($x = 0$). The three curves correspond to the following three geometries: (*A*) an unbranched tree of length $L = \lambda$ (λ is the space constant); (*B*) an unbranched tree of length 2λ; (*C*) the branched tree for which each branch has length $L = \lambda$. When the synaptic input is close to the recording point, the geometry distal to the synapse has little effect on the peak voltage. However, as the input recedes from the recording point, the magnitude (and, as we shall see, the time-course) of the recorded PSP becomes more influenced by the nature of the distal geometry. Some of the injected current spreads toward the periphery; the amount is small when the synapse is near $x = 0$, but it becomes a larger fraction of the total as D increases. The exact fraction, as can be seen from Fig. 10, depends on the details of the peripheral current pathways. For example, at its peak more current moves distally when the tree branches, thus reducing the amount moving toward $x = 0$. Hence, a smaller peak value is recorded for a given synaptic site for the branched vs. an unbranched system.

Because we are dealing with time-varying currents and because it takes time and current to charge the membrane capacitances, we expect the time-course of the recorded PSP also to be correlated with the dendritic geometry. Rall (1967) has defined a number of shape indices with which to analyze the PSP time-course. The two that will be used here are t_0, the time of the peak amplitude (measured from $t = 0$), and $\Delta t_{1/2}$, the half-width, which is defined as the width of the PSP at half of peak amplitude. Fig. 11 displays a plot of half-width vs. peak time for the three geometries whose v_m vs. D graphs were just discussed. It should be noted first that curves *A* and *B* for the unbranched geometries agree rather closely with results obtained by Rall et al. (1967. cf., their Fig. 6) using a compartmental model.[6] Consequently, the *G*-function formalism does produce correct values for $v(t)$. The second point of interest is that the distal geometry affects the time-course of the transient voltage change in a complicated way: especially for the more distal values of D, both the peak time and half-width depend on the distal branching pattern. A more thorough discussion of this, including what happens as the input site moves onto the peripheral branches, will be presented elsewhere (Horwitz, 1981). However, we can conclude in agreement with Rall (1967) that the location of a

[6]There are small differences due to the fact that Rall et al. used an injected current with an initial spread in time, that one of their branches was 1.8λ rather than 2.0λ in length, and that their definition of peak time differs slightly from the one used by me.

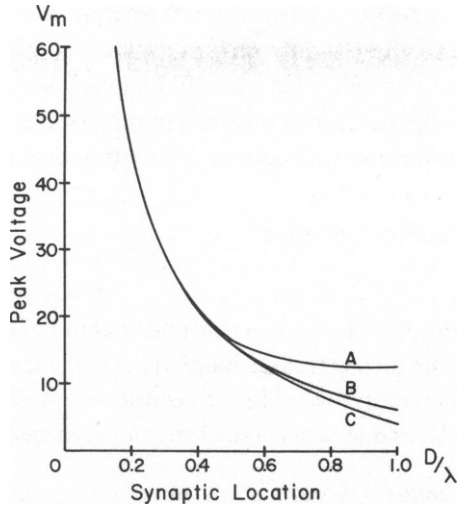

FIGURE 10 A plot of peak voltage (v_m) vs. distance (D) between the synaptic input and the recording point. *A* corresponds to an unbranched tree of length $L = \lambda$ (Fig. 3), *B* to an unbranched tree of length $L = 2\lambda$, and *C* to the branched tree (Fig. 4 *b*) for which each branch has length $L = \lambda$. In the last case the synaptic input is on the primary branch. For all three configurations the recording point is at the extreme left ($x = 0$). The units are the same as in Fig. 9.

synaptic input cannot be inferred from the PSP shape alone. Moreover, even in a purely linear system, dendritic branching can have a marked effect on how a synapse, a given physical distance from a specified location, is "perceived" at that point, and thus, on how the integration of many synapses takes place.

It should be noted that the above results were obtained for a tree in which all branches were

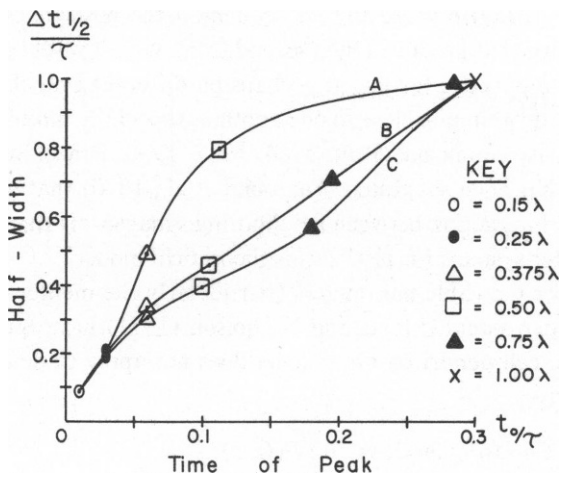

FIGURE 11 A plot of half-width ($\Delta t_{1/2}$) vs. peak time (t_0) for the three geometries examined in Fig. 10. The points indicated by the symbols correspond to the same physical location for the synaptic input: $D = 0.15\lambda$ (○); $D = 0.25\lambda$ (●); $D = 0.375\lambda$ (△); $D = 0.50\lambda$ (□), $D = 0.75\lambda$ (▲), $D = 1.00\lambda$ (X). Note that time is measured in units of the time constant.

of equal diameter. If we have different diameters, the details, but not the substance, of these results will change. Also, all these numerical results were obtained for the case of a delta function current input. If the current input has a finite time-course one further integration of Eq. 27 is required. Essentially, the results obtained in this section are for the time-course and amplitudes of the transfer functions associated with particular synapse-recording location-geometry triads.

DISCUSSION

The analysis presented here has centered on several definite geometries, none of which is particularly complicated from a structural point of view. It is therefore crucial to address the question of how far this method can be taken, to consider how these theoretical expressions can be tested experimentally, and to reflect on what can be learned from such tests.

More Than One Input

Our calculations have been concerned with a single input, and with the propagation of a single postsynaptic potential produced by it. The model we used assumes linear (passive) cable properties; in addition, the inverse Laplace transformation is a linear mathematical operator. Therefore, the transient potential at $x = 0$ in response to N inputs at different locations on the dendritic tree is given by

$$v(0, t) = \sum_{i=1}^{n} v_i(0, t) \tag{80}$$

where $v_i(0, t)$ is the potential at $x = 0$ due to the ith synaptic input. Each of the individual potentials is calculable by the method discussed above.

This principle of superposition ignores two kinds of nonlinearities found in dendritic systems. The first is that the driving potential for synaptic currents depends on the transmembrane potential difference, and consequently, the postsynaptic potential produced by one input can change that produced by a second from what it would have been had the first been absent. If these inputs are far apart, perhaps on different branches, this effect is small and can be ignored; but for inputs close to one another, especially inhibitory PSPs, substantial deviations from linearity can occur (Rall, 1964, 1967, 1970; Rinzel and Rall, 1974; Barrett and Crill, 1974*b*). It has been suggested (Diamond et al., 1970) that dendritic spines reduce this type of nonlinear interaction between neighboring synapses. If this is the case, then spiny neurons offer the better systems for testing this theoretical model.

It is also possible for the cable parameters (particularly the membrane conductance G) to be explicitly voltage dependent. Llinas and Nicholson (1971) have reported observing spike potentials in Purkinje cell dendrites. Our model does not apply to dendritic trees possessing this kind of nonlinearity.

Criteria for Choosing $A(D, s)$ and $F(G, s)$

To see how general the method we have developed can be made, we must delineate the way one goes about choosing the expressions for $A(D, s)$ and $F(G, s)$. We had defined $A(D, s)$ as the Laplace transformation of $a(D, t)$—the factor that depends primarily on the location of

the input to the dendritic system. $F(G, s)$ is the Laplace transform of the geometry factor, $f(G, t)$. From the results obtained in the previous section we can conclude that $a(D, t)$ [or $A(D, s)$] will depend upon two features: (*a*) the location of the synaptic input on a given branch, and (*b*) the branching pattern distal to the input.[7] Therefore, the expression for $a(D, t)$ will not be totally independent of the geometry. For example, $a(D, t)$ is the same for the geometry of Fig. 4 *a* as it is for the geometry of Fig. 5 *a*. Similarly, the same expression for $a(D, t)$ pertains to Figs. 4 *b* and Fig. 5 *c*. Consequently, for a new geometry $a(D, t)$ will have to be worked out only when the input is on the primary branch; when the input is on a secondary, tertiary, etc. branch, a previously derived expression will hold.

Therefore, because $R(x, s)$, the factor corresponding to the recording location is always the same [$R(x, s) = Z_c \cosh \gamma x$], the procedure for choosing the correct expressions for $A(D, s)$ and $F(G, s)$ consists of the following: (*a*) if the input is not on the primary branch, choose for $A(D, s)$ the appropriate previously derived expression; what remains in the expression $V(x, s)/[Z_c \cosh \gamma x\, I_{sy}(s)]$ is $F(G, s)$; (*b*) if the input is on the main branch, $F(G, s) = 1$ and $A(D, s) = V(x, s)/[Z_c \cosh \gamma x\, I_{sy}(s)]$.

We still must detail the criteria used for the expressions we have derived. That is, how did we choose the particular forms for $A(D, s)$ that we did, such as those given by Eq. 22? Two criteria predominated. First, $A(D, s)$ and $F(G, s)$ must be chosen so that their inverse Laplace transforms could be found in analytical form. This restricted the potential choices considerably. Second, $A(D, s)$ was selected in such a way that the remaining expression for $F(G, s)$ would exhibit certain symmetries in the way some of the branch lengths appear. Thus, for the geometry of Fig. 4 *a* we have from Eq. 23 that $F(G, s)$ is symmetric in L_1 and L_2 (assuming $Z_{c_1} = Z_{c_2}$); i.e.,

$$F(L_1, L_2, s) = F(L_2, L_1, s). \tag{81}$$

Similarly, for the geometry of Fig. 5 from Eqs. A6, A26 and A41 we see that

$$F(L_3, L_4, s) = F(L_4, L_3, s). \tag{82}$$

These invariances say that the mathematical form for $F(G, s)$ shouldn't depend on the location of the input; any geometrical symmetries in the geometry, such as, for example, L_3 and L_4 of Fig. 5 both being terminal tertiary branches, should be reflected mathematically in the expression for $F(G, s)$.

Although we have examined explicitly only a few geometries, it appears that our method can be employed to study geometries with higher order branching. The Butz-Cowan rules (taking all the $Z_c s$ and γs as equal) essentially allow one to write

$$V(0, s) = \frac{Z_c N(\sigma_D, \eta_D)}{D(\sigma, \eta)} I_{sy}(s) \tag{83}$$

where N is a polynomial in the variables $\sigma_D = \sinh \gamma(L - D)$ and $\eta_D = \cosh \gamma(L - D)$, and D is a polynomial in the variables $\sigma = \sinh \gamma L$; and $\eta = \cosh \gamma L$. We can factor these polynomials

[7]The particular expression one gets for $a(D, t)$ also depends on the choice of boundary conditions, a point which will be discussed below.

so that

$$V(0, s) = KZ_c \frac{(\sigma_D + \alpha_1\eta_D)(\sigma_D + \alpha_2\eta_D) \cdot \cdot \cdot (\sigma_D + \alpha_n\eta_D)}{(\sigma + \beta_1\eta)(\sigma + \beta_2\eta) \cdot \cdot \cdot (\sigma + \beta_k\eta)}. \tag{84}$$

K is an overall normalization constant; inverting, we get

$$v(0, t) = Kr(0, t) * \{G_{1\beta_1;s}(t) + \alpha_1 G_{1\beta_1;c}(t)\} * \{G_{1\beta_2;s}(t) + \alpha_2 G_{1\beta_2;c}(t)\} * \cdot \cdot \cdot * i_{sy}(t). \tag{85}$$

As before, the asterisk means convolution. The advantage of introducing the factors $a(D, t)$ and $f(G, t)$ is that they permit us to analyze the convolution product of Eq. 85 in a systematic way. It would be useful to have a procedure for specifying the numbers α_i, β_i and K of Eq. 85 for any arbitrary geometry in the same way that the rules of Butz-Cowan allow us to specify the expression for $V(x, s)$ for any geometry.

Different Boundary Conditions

It was assumed in our evaluation of the specific primitive integrals in a previous section that all branches had sealed end terminations. The Butz-Cowan (1974) graphical calculus, however, allows one to use other boundary conditions. Some terminations could be open circuit (killed end); we could even have a branch ending in a cell body (lumped soma boundary condition). If some or all of the terminations are of the killed and variety, the expression for $V(x, s)$ would differ from the corresponding expression with sealed end terminations in a simple way: some of the hyperbolic cosines would be hyperbolic sines and vice-versa (see Butz-Cowan [1974] for a more detailed discussion). The particular expressions that we have derived for $a(D, t)$ and $f(G, t)$ would be different, but they could still be written using the G-function formalism. We shall illustrate this using the geometry of Fig. 4 *a*. The Butz-Cowan rules produce the following expression for $V(x, s)$ when L_0 terminates in a sealed end, and L_1 and L_2 each terminate with a killed end:

$$V(x, s) = \frac{Z_{c_0}Z_{c_1}Z_{c_2} \cosh \gamma_0 x \sinh \gamma_1(L_1 - D) \sinh \gamma_2 L_2}{\left[\begin{array}{l} Z_{c_0}Z_{c_1} \cosh \gamma_0 L_0 \sinh \gamma_1 L_1 \cosh \gamma_2 L_2 \\ + Z_{c_0}Z_{c_2} \cosh \gamma_0 L_0 \cosh \gamma_1 L_1 \sinh \gamma_2 L_2 \\ + Z_{c_1}Z_{c_2} \sinh \gamma_0 L_0 \sinh \gamma_1 L_1 \sinh \gamma_2 L_2 \end{array}\right]} I_{sy}(s). \tag{86}$$

We choose

$$R(0, s) = Z_{c_0} = \frac{R}{\gamma_0} \tag{87}$$

$$A(D, s) = \frac{\sinh \gamma_1(L_1 - D)}{\sinh \gamma_1, L_1} \tag{88}$$

$$F(G, s) = \frac{Z_{c_1}Z_{c_2} \sinh \gamma_1 L_1 \sinh \gamma_2 L_2}{\left[\begin{array}{l} Z_{c_0}Z_{c_1} \cosh \gamma_0 L_0 \sinh \gamma_1 L_1 \cosh \gamma_2 L_2 \\ + Z_{c_0}Z_{c_2} \cosh \gamma_0 L_0 \cosh \gamma_1 L_1 \sinh \gamma_2 L_2 \\ + Z_{c_1}Z_{c_2} \sinh \gamma_0 L_0 \sinh \gamma_1 L_1 \sinh \gamma_2 L_2 \end{array}\right]} \tag{89}$$

If, as before, we assume $\gamma_i = \gamma$ and $Z_{c_i} = Z_c$ $(i = 0, 1, 2)$, then for the case where all the lengths are equal, we have

$$a(D, t) = G_{10;s}(L - D, t) \tag{90}$$

$$f(G, t) = \tfrac{1}{2}\{G_{1i\sqrt{2};c}(0, t) + G_{1-i\sqrt{2};c}(0, t)\}. \tag{91}$$

If the only killed end is on the branch of length L_2, then the expressions for $R(0, s)$ and $A(D, s)$ remain unchanged from those they had for sealed ends (i.e., Eqs. 21 and 22). The only change is in the form of $F(G, s)$:

$$F(G, s) = \frac{Z_{c_1} Z_{c_2} \cosh \gamma_1 L_1 \sinh \gamma_2 L_2}{\left[\begin{array}{l} Z_{c_0} Z_{c_1} \cosh \gamma_0 L_0 \cosh \gamma_1 L_1 \cosh \gamma_2 L_2 \\ + Z_{c_0} Z_{c_2} \cosh \gamma_0 L_0 \sinh \gamma_1 L_1 \sinh \gamma_2 L_2 \\ + Z_{c_1} Z_{c_2} \sinh \gamma_0 L_0 \cosh \gamma_1 L_1 \sinh \gamma_2 L_2 \end{array}\right]}. \tag{92}$$

For the equal length case and making the standard assumptions, we find

$$a(D, t) = G_{01;c}(L - D, t) \tag{93}$$

$$f(G, t) = \tfrac{1}{4}\{G_{1(i/\sqrt{2});c}(0, t) + G_{1-(i/\sqrt{2});s}(0, t)\}. \tag{94}$$

This method of analysis can therefore be used for systems in which different boundary terminations occur in different parts of the dendritic tree.

Unequal Diameters

To apply this model to neurons whose behavior can be determined experimentally, the correction terms to the primitive integrals will require evaluation. The most important corrections will involve dendritic systems whose branches have varying diameters. The factors which depend on the branch diameter are the membrane conductance G, the core resistance R, and the membrane capacitance C.

$$G = \frac{\pi d}{R_m} \tag{95}$$

$$R = \frac{4\rho}{\pi d^2} \tag{96}$$

$$C = \pi d C_m \tag{97}$$

where R_m is the membrane resistance of a branch unit surface area, C_m is the membrane capacitance per unit surface area, ρ is the intracellular resistivity, and d is the diameter of the branch. The space constant λ, the quantity γ and the characteristic impedance Z_c consequently all acquire a dependence on d, although the time constant τ does not:

$$\lambda = \sqrt{\frac{R_m}{4\rho}}\, d^{1/2} \tag{98}$$

$$\gamma = \sqrt{\frac{4\rho(s\tau + 1)}{R_m}}\, d^{-1/2} \tag{99}$$

$$Z_c = \frac{1}{\pi}\sqrt{\frac{4\rho R_m}{s\tau + 1}}\, d^{-3/2}. \tag{100}$$

Therefore, we cannot set equal all the $\lambda_i s$, $\gamma_i s$, or $Z_{c_i} s$. Thus, the geometry factor $F(G, s)$ will be a function of the different branch diameters. This can be expressed symbolically as

$$F(G, s) = F(d_0, d_1, d_2, \ldots, d_n, s). \tag{101}$$

One standard approximation technique that can be employed uses the Taylor expansion (in $n - 1$ variables):

$$\begin{aligned} F(G, s) = F(d_0, d_0, \ldots, s) &+ (d_1 - d_0)\left(\frac{\partial F}{\partial d_1}\right)_{d_i = d_0} \\ &+ (d_2 - d_0)\left(\frac{\partial F}{\partial d_2}\right)_{d_i = d_0} + \cdots + (d_n - d_0)\left(\frac{\partial F}{\partial d_n}\right)_{d_i = d_0} \\ &+ O[(d_i - d_0)^2]. \end{aligned} \tag{102}$$

Thus, the correction terms to Eq. 27 will incorporate the first-order terms of Eq. 102, and possibly the higher order terms if needed.

We shall illustrate the effects on the transient voltage of a dendritic tree whose branches have unequal diameters by using the simple geometry of Fig. 4 *a*. Let each of the diameters of the secondary branches by some fraction of primary branch diameter, i.e., $d_1 = f_1 d_0$, $d_2 = f_2 d_0$. Then to first order,

$$F(G, s) = F_0(G, s) - (1 - f_1) d_0 \left(\frac{\partial F}{\partial d_1}\right)_{d_i = d_0} - (1 - f_2) d_0 \left(\frac{\partial F}{\partial d_2}\right)_{d_i = d_0}. \tag{103}$$

$F_0(G, s)$ is the expression for $F(G, s)$ when all the diameters are equal. For example, for the case where all lengths are equal, $F_0(G, s)$ is given by Eq. 43; the two partial derivatives are obtained by combining Eqs. 98–100 with Eq. 23, and then differentiating. The inverse transform can then be found and inserted into Eq. 27. Fig. 12 exhibits the results of the ensuing numerical evaluation for three cases: (1) $f_1 = f_2 = 0.5$ which corresponds to thin branches; (2) $f_1 = f_2 = 0.63$ which corresponds to the case where the system obeys the 3/2 rule; (3) $f_1 = f_2 = 0.8$. Plotted along with these is the equal diameter tree. In all four cases the input site is a quarter of the way up a secondary branch. Two factors contribute to the increase in peak amplitude as the secondary diameters decrease. First, the peripheral resistance has increased, thus allowing more of the injected current to flow to $x = 0$. Second, the total membrane capacity has also decreased; the same amount of input current into a smaller capacitance results in a larger voltage amplitude. Notice that this procedure allows us to consider any particular set of diameter relationships; we are not forced to use a specific one, such as given by the 3/2 rule. Obviously, the smaller f_1 and f_2 are, the more likely higher order terms will be required.

Applications

Previous analytical treatments of branching dendritic systems have avoided, for the most part, treating the branches individually. Besides Butz and Cowan (1974), only Rall and Rinzel 1973; Rinzel and Rall, 1974) have dealt with a single input on a single branch. My approach to this problem is best viewed as complementing the Rall-Rinzel treatment. By and large their effort was directed at evaluating the attenuation and delay characteristics of a depolarization peak as it spreads throughout a model neuron in which the arborization possessed a high

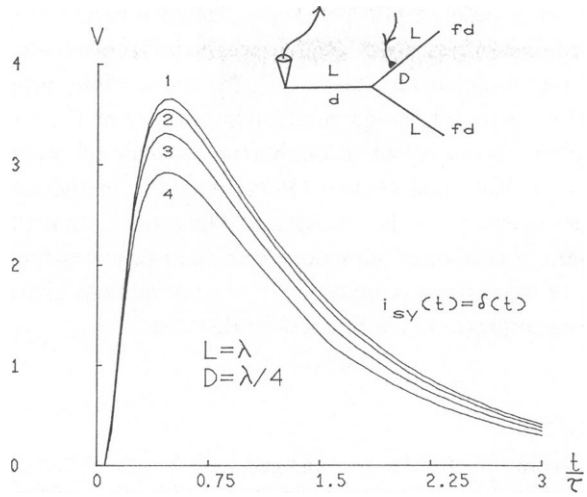

FIGURE 12 A plot of $v(0, t)$ vs. t for the branched tree shown in the *inset*. The secondary branches each have a diameter which is a fraction f of the primary branch diameter. All three branches have length $L = \lambda$. The synaptic input for each case is located on a secondary branch, a distance $D = \lambda/4$ from the bifurcation. The units are the same as in Fig. 9. The four cases shown correspond to (*1*) thin branch case ($f = 0.5$); (*2*) 3/2 rule case ($f = 0.63$); (*3*) $f = 0.8$; (*4*) equal diameter case ($f = 1$).

degree of symmetry.[8] My method focuses primarily on how a change in the branching pattern affects the transient voltage at a specified point in the tree. Therefore, even though the particular geometries we have examined are relatively simple, we now can investigate in a systematic fashion the way in which the potential at a specified point, for an input somewhere else, depends upon such geometrical parameters as (*a*) the number of sister branches, (*b*) the branch lengths, (*c*) whether or not the dendrite bifurcates at a point distal to the input, and (*d*) given such a bifurcation, the lengths of the daughter branches. An example of this kind of analysis entails the numerical evaluation of the primitive integrals for the arrangements shown in Figs. 4 *a*, 5 *c*, and 6 *a*. A subsequent paper will deal with the results of that analysis.

Most neurons have dendritic arborizations more ramified than the model systems considered in this paper. However, it is possible by using laser microbeam irradiation to achieve precise and highly localized neurite transections of neurons in tissue culture (Rieske et al., 1977; Rieske and Kreutzberg, 1978; Higgins et al., 1980); indeed, the lasers that were used in these studies can be focused to 0.7μm. This method provides the possibility of simplifying the dendritic tree of a neuron until its geometry approximates one of the model systems. Conventional intracellular recording techniques can then be used to check the validity of the assumptions in the model, particularly the assumption that the dendritic cable only behaves passively. Such studies are currently under way in our laboratory.

Concluding Remarks

Given a branched dendritic system with one synaptic input at a particular location, how is that synaptic input "perceived" at some other point? By perceived I mean time-course and

[8] They do indicate how some of the geometrical constraints in their method can be relaxed.

amplitude of the resulting postsynaptic potential. The parameters that govern this can be placed into one of three categories: (*a*) the cable properties—core resistance (R), membrane capacitance (C) and membrane conductance (G); (*b*) the synaptic properties—the strength and time-course of the input; (*c*) the geometrical properties of the tree—for example, the lengths of the branches, their respective diameters, number of orders of branching, etc. Combining the results of Butz and Cowan (1974) with the method outlined in this paper allows the last of these categories to be considered. The crucial point that emerged from the analysis presented here is that the G-function formalism provides the appropriate way for treating the behavior of these systems analytically; the G-functions give us a precise language for talking about the structure-function relation for dendritic trees.

APPENDIX A

In this appendix we list expressions for the input and geometry factors, $a(D, t)$ and $f(G, t)$, respectively, for a number of symmetric geometries corresponding to the dendritic configurations shown in Figs. 5 and 6. The associated primitive integrals are obtained by inserting these expressions into Eq. 27. The expression for the recording location factor, $r(x, t)$, is given by Eq. 39. As pointed out in the main body of the paper, there are in principle an infinite number of primitive integral geometries for these trees; thus, we shall provide below only a few illustrative cases for each configuration.

In each case we make the standard assumptions: $Z_{c_i} = Z_c$ and $\gamma_i = \gamma$ ($i = 0, 1, 2, 3, 4$), all branch diameters equal. For each we list $A(D, s)$, $F(G, s)$, $a(D, t)$ and $f(G, t)$.

1. Tree With Two Bifurcations (see Fig. 5)

There are four locations for the synaptic input: on L_3 (or L_4), on L_2, on L_1, or on L_0. We treat each separately.

A. INPUT ON L_3 (FIG. 5*a*): The rules of Butz-Cowan (1974) enable us to write down the expression for $V(0, s)$:

$$V(0, s) = \frac{Z_c \cosh \gamma L_2 \cosh \gamma L_4 \cosh \gamma (L_3 - D)}{\Delta_2} I_{sy}(s) \tag{A1}$$

with

$$\Delta_2 = \Delta_a(\cosh \gamma L_3 \sinh \gamma L_4 + \sinh \gamma L_3 \cosh \gamma L_4) + \Delta_b \sinh \gamma L_3 \sinh \gamma L_4 \tag{A2}$$

and

$$\Delta_a = \sinh \gamma L_0 \sinh \gamma L_1 \cosh \gamma L_2 + \sinh \gamma L_0 \cosh \gamma L_1 \sinh \gamma L_2 + \cosh \gamma L_0 \sinh \gamma L_1 \sinh \gamma L_2 \tag{A3}$$

$$\Delta_b = \cosh \gamma L_0 \cosh \gamma L_1 \sinh \gamma L_2 + \cosh \gamma L_0 \sinh \gamma L_1 \cosh \gamma L_2 + \sinh \gamma L_0 \cosh \gamma L_1 \cosh \gamma L_2. \tag{A4}$$

We choose

$$A(D, s) = \frac{\cosh \gamma (L_3 - D)}{\cosh \gamma L_3} \tag{A5}$$

$$F(G, s) = \frac{\cosh \gamma L_2 \cosh \gamma L_3 \cosh \gamma L_4}{\Delta_2}. \tag{A6}$$

Notice that $A(D, s)$ has precisely the same form as was the case when we had one bifurcation and the input was on the peripheral branch (p. 168).

(*a*) $L_i = L$ $(i = 0, 1, 2, 3, 4)$:

$$A(D, s) = \frac{\cosh \gamma(L - D)}{\cosh \gamma L} \tag{A7}$$

$$a(D, t) = G_{01;c}(L - D, t) \tag{A8}$$

$$F(G, s) = \frac{1}{9} \frac{\cosh \gamma L}{\sinh \gamma L} \frac{1}{\sinh^2 \gamma L} \tag{A9}$$

$$f(G, t) = \tfrac{1}{9} G_{10;c}(L, t) * G_{10;c}(0, t) * G_{10;c}(0, t). \tag{A10}$$

The asterick in Eq. A10, as before, means convolution.

(*b*) $L_3 = 2L$, *all other* $L_i = L$:

$$A(D, s) = \frac{\cosh \gamma(2L - D)}{\cosh 2\gamma L} \tag{A11}$$

$$a(D, t) = G_{01;c}(2L - D, t) \tag{A12}$$

$$F(G, s) = \frac{1}{75 \cosh \gamma L} \left\{ \frac{9}{\sinh \gamma L} + \frac{5}{\sinh^3 \gamma L} - 2 \left[\frac{1}{\sinh \gamma L + i\sqrt{5} \cosh \gamma L} + \frac{1}{\sinh \gamma L - i\sqrt{5} \cosh \gamma L} \right] \right\} \tag{A13}$$

$$\begin{aligned} f(G, t) = {} & \tfrac{1}{75} G_{01;c}(0, t) * \{9G_{10;c}(0, t) \\ & + 5G_{10;c}(0, t) * G_{10;c}(0, t) * G_{10;c}(0, t) \\ & - 2[G_{1i\sqrt{5};c}(0, t) + G_{1-i\sqrt{5};c}(0, t)]\}. \end{aligned} \tag{A14}$$

(*c*) $L_4 = 2L$, *all other* $L_i = L$: $a(D, t)$ is given by Eq. A8, $f(G, t)$ by Eq. A14.
(*d*) $L_1 = 2L$, *all other* $L_i = L$: $a(D, t)$ is given by Eq. A8.

$$F(G, s) = \frac{1}{98} \left\{ -\frac{2}{\sinh \gamma L} + \frac{7}{\sinh^3 \gamma L} + \frac{9}{2} \left[\frac{1}{\sinh \gamma L + i\sqrt{3.5} \cosh \gamma L} + \frac{1}{\sinh \gamma L - i\sqrt{3.5} \cosh \gamma L} \right] \right\}. \tag{A15}$$

$$\begin{aligned} f(G, t) = {} & \tfrac{1}{98}\{-2G_{10;c}(0, t) + 7G_{10;c}(0, t) * G_{10;c}(0, t) * G_{10;c}(0, t) \\ & + \tfrac{9}{2} [G_{1i\sqrt{3.5};c}(0, t) + G_{1-i\sqrt{3.5};c}(0, t)]\}. \end{aligned} \tag{A16}$$

(*e*) $L_3 \to \infty$, *all other* $L_i = L$:

$$A(D, s) = e^{-\gamma D} \tag{A17}$$

$$a(D, t) = g(D, t) \tag{A18}$$

$$F(G, s) = \frac{\cosh \gamma L}{3 \sinh^2 \gamma L(\sinh \gamma L + 2 \cosh \gamma L)} \tag{A19}$$

$$f(G, t) = \tfrac{1}{6}\, G_{10;c}(0, t) * [G_{10;c}(0, t) - G_{12;c}(0, t)]. \tag{A20}$$

(f) $L_4 \to \infty$, *all other* $L_i = L$: $a(D, t)$ is given by Eq. A8, $f(G, t)$ by Eq. A20.
(g) $L_2 \to \infty$, $L_3 \to \infty$, *all other* $L_i = L$: $a(D, t)$ is given by Eq. A18.

$$F(G, s) = 1.43 \frac{\cosh \gamma L}{\sinh \gamma L}\left(\frac{1}{1.43 \sinh \gamma L + \cosh \gamma L}\right)\left(\frac{1}{\sinh \gamma L + 4.30 \cosh \gamma L}\right). \tag{A21}$$

$$f(G, t) = 1.43\, G_{1,4.30;c}(0, t) * [G_{10;c}(0, t) - 1.43\, G_{1.43,1;c}(0, t)]. \tag{A22}$$

B. INPUT ON L_2 (FIG. 5 *b*)

$$V(0, s) = \frac{Z_c \Delta_3 \cosh \gamma(L_2 - D)}{\Delta_2} I_{sy}(s) \tag{A23}$$

where Δ_2 is given by Eq. A2, and

$$\Delta_3 = \sinh \gamma L_1 \cosh \gamma L_3 \sinh \gamma L_4 + \sinh \gamma L_1 \sinh \gamma L_3 \cosh \gamma L_4 + \cosh \gamma L_1 \cosh \gamma L_3 \cosh \gamma L_4. \tag{A24}$$

We choose

$$A(D, s) = \frac{\cosh \gamma(L_2 - D)}{\cosh \gamma L_2} \tag{A25}$$

$$F(G, s) = \frac{\Delta_3 \cosh \gamma L_2}{\Delta_2}. \tag{A26}$$

(a) $L_i \equiv L$ $(i = 0, 1, 2, 3, 4)$: $a(D, t)$ is given by Eq. A8.

$$F(G, s) = \frac{2}{9 \sinh \gamma L} + \frac{1}{9 \sinh^3 \gamma L} \tag{A27}$$

$$f(G, t) = \tfrac{2}{9} G_{10;c}(0, t) + \tfrac{1}{9} G_{10;c}(0, t) * G_{10;c}(0, t) * G_{10;c}(0, t). \tag{A28}$$

(b) $L_3 = 2L$, *all other* $L_i = L$: $a(D, t)$ is given by Eq. A12.

$$F(G, s) = \frac{1}{75}\left[\frac{19}{\sinh \gamma L} + \frac{5 \cosh^2 \gamma L}{\sinh^3 \gamma L} + \frac{3}{\sinh \gamma L + i\sqrt{5} \cosh \gamma L} + \frac{3}{\sinh \gamma L - i\sqrt{5} \cosh \gamma L}\right] \tag{A29}$$

$$f(G, t) = \tfrac{1}{75}\,[19 G_{10;c}(0, t) + 5 G_{10;c}(L, t) * G_{10;c}(L, t) * G_{10;c}(0, t) + 3 G_{1i\sqrt{5};c}(0, t) + 3 G_{1-i\sqrt{5};c}(0, t)]. \tag{A30}$$

(c) $L_4 = 2L$, *all other* $L_i = L$: $a(D, t)$ is given by Eq. A8, $f(G, t)$ by Eq. A30.

(*d*) $L_1 = 2L$, *all other* $L_i = L$: $a(D, t)$ is given by Eq. A8.

$$F(G, s) = \frac{1}{14}\frac{\cosh \gamma L}{\sinh \gamma L}\left\{\frac{1}{\sinh^2 \gamma L} - \frac{33}{4}\left[\frac{\sinh \gamma L - \dfrac{i \cosh \gamma L}{\sqrt{3.5}}}{\sinh \gamma L + i\sqrt{3.5}\cosh \gamma L} + \frac{\sinh \gamma L + \dfrac{i \cosh \gamma L}{\sqrt{3.5}}}{\sinh \gamma L - i\sqrt{3.5}\cosh \gamma L}\right]\right\} \tag{A31}$$

$$\begin{aligned} F(G, t) = {} & \tfrac{1}{14}\, G_{10;c}(L,t) * \{G_{10;c}(0, t) * G_{10;c}(0, t) \\ & - \tfrac{33}{4}[G_{1i\sqrt{3.5};s}(L, t) - (i/\sqrt{3.5})\, G_{1i\sqrt{3.5};c}(L, t) \\ & + G_{1-i\sqrt{3.5};s}(L, t) + (i/\sqrt{3.5}) G_{1-i\sqrt{3.5};c}(L, t)]\}. \end{aligned} \tag{A32}$$

(*e*) $L_3 \to \infty$, *all other* $L_i = L$ *(or* $L_4 \to \infty$, *all other* $L_i = L$*)*: $a(D, t)$ is given by Eq. A8.

$$F(G, s) = [1/3\,(\sinh \gamma L + 2\cosh \gamma L)]\left[1 + \frac{\cosh \gamma L}{\sinh \gamma L} + \left(\frac{\cosh \gamma L}{\sinh \gamma L}\right)^2\right] \tag{A33}$$

$$f(G, t) = \tfrac{1}{4}\, G_{12;c}(0, t) + \tfrac{1}{12}\, G_{10;c}(0, t) + \tfrac{1}{6}\, G_{10;c}(0, t) * G_{10;c}(L, t). \tag{A34}$$

(*f*) $L_2 \to \infty$, $L_3 \to \infty$, *all other* $L_i = L$ *(or* $L_2 \to \infty$, $L_4 \to \infty$, *all other* $L_i = L$*)*: $a(D, t)$ is given by Eq. A18.

$$F(G, s) = \frac{\cosh \gamma L}{\sinh \gamma L + 4.3\cosh \gamma L}\left[\frac{1.43 \coth 2\gamma L}{1.43 \sinh \gamma L + \cosh \gamma L} + \frac{1}{\sinh \gamma L + 0.7 \cosh \gamma L}\right] \tag{A35}$$

$$\begin{aligned} f(G, t) = {} & 0.28\,[G_{1,0.7;c}(0, t) - G_{1,4.3;c}(0, t)] \\ & + 1.43\, G_{10;c}(2L, t) * [0.28\, G_{1.43,1;c}(0, t) - 0.19\, G_{1,4.3;c}(0, t)]. \end{aligned} \tag{A36}$$

C. INPUT ON L_1 (FIG. 5*c*)

$$V(0, s) = \frac{Z_c \Delta_4 \cosh \gamma L_2}{\Delta_2} I_{sy}(s) \tag{A37}$$

where Δ_2 is given by Eq. A2, and

$$\begin{aligned} \Delta_4 = {} & \sinh \gamma(L_1 - D)\cosh \gamma L_3 \sinh \gamma L_4 \\ & + \sinh \gamma(L_1 - D)\sinh \gamma L_3 \cosh \gamma L_4 + \cosh \gamma(L_1 - D)\cosh \gamma L_3 \cosh \gamma L_4. \end{aligned} \tag{A38}$$

Define

$$\begin{aligned} D_1 = {} & \cosh \gamma L_1 \cosh \gamma L_3 \sinh \gamma L_4 \\ & + \cosh \gamma L_1 \sinh \gamma L_3 \cosh \gamma L_4 \\ & + \sinh \gamma L_1 \cosh \gamma L_3 \cosh \gamma L_4 \end{aligned} \tag{A39}$$

and choose

$$A(D, s) = \frac{\Delta_4}{D_1} \tag{A40}$$

and

$$F(G, s) = \frac{D_1 \cosh \gamma L_2}{\Delta_2}. \tag{A41}$$

These choices for $A(D, s)$ and $F(G, s)$ are the most appropriate. In particular, $A(D, s)$ has precisely the same mathematical form as it did for the geometry of Fig. 4 *b* (see Eq. 67). Thus, the expressions for $a(D, t)$ are also the same. This way of choosing $A(D, s)$ is examined more closely in the Discussion section of the paper.

(*a*) *$L_i = L$ ($i = 0, 1, 2, 3, 4$):* $a(D, t)$ is given by Eq. 71.

$$F(G, s) = \frac{1}{3 \sinh \gamma L} \frac{\cosh \gamma L}{\sinh \gamma L} \tag{A42}$$

$$f(G, t)\ \tfrac{1}{3}\, G_{10;c}(0, t) * G_{10;c}(L, t). \tag{A43}$$

(*b*) *$L_3 = L_4 = 2L$, all other $L_i = L$:* $a(D, t)$ is given by Eq. 77.

$$F(G, s) = \frac{1}{24}\left(\frac{5 \cosh \gamma L}{\sinh^2 \gamma L} + \frac{1}{\cosh \gamma L}\right) \cdot \left(\frac{\sinh \gamma L + \dfrac{i \cosh \gamma L}{\sqrt{2}}}{\sinh \gamma L + i\sqrt{2} \cosh \gamma L} + \frac{\sinh \gamma L - \dfrac{i \cosh \gamma L}{\sqrt{2}}}{\sinh \gamma L - i\sqrt{2} \cosh \gamma L}\right) \tag{A44}$$

$$f(G, t) = \tfrac{1}{24}[5G_{10;c}(L, t) * G_{10;c}(0, t) + G_{01;c}(0, t)] * [G_{1i\sqrt{2};s}(L, t) + \frac{i}{\sqrt{2}} G_{1i\sqrt{2};c}(L, t) + G_{1-i\sqrt{2};s}(L, t) - \frac{i}{\sqrt{2}} G_{1-i\sqrt{2};c}(L, t)]. \tag{A45}$$

(*c*) *$L_3 \to \infty$, all other $L_i = L$ (or $L_4 \to \infty$, all other $L_i = L$):* $a(D, t)$ is given by Eq. 73.

$$F(G, s) = \frac{2}{3} \frac{\coth \gamma L}{3 \sinh \gamma L + 2 \cosh \gamma L} + \frac{1}{3} \frac{\coth^2 \gamma L}{3 \sinh \gamma L + 2 \cosh \gamma L} \tag{A46}$$

$$f(G, t)\ \tfrac{1}{4}\, G_{10;c}(0, t) - \tfrac{1}{4}\, G_{12;c}(0, t) + \tfrac{1}{6}\, G_{10;c}(0, t) * G_{10;c}(L, t) \tag{A47}$$

(*d*) *$L_2 \to \infty$, all other $L_i = L$:* $a(D, t)$ is given by Eq. 71.

$$F(G, s) = \frac{3 \coth \gamma L}{4 \sinh \gamma L + 5 \cosh \gamma L} \tag{A48}$$

$$f(G, t) = \tfrac{3}{5}\, G_{10;c}(0,t) - \tfrac{12}{5}\, G_{45;c}(0, t). \tag{A49}$$

D. INPUT ON L_0 (FIG. 5 *d*)

$$V(0, s) = \frac{Z_c \Delta_5}{\Delta_2} I_{sy}(s) \tag{A50}$$

where Δ_2 is given by Eq. A2, and

$$\Delta_5 = \Delta_{51}(\sinh \gamma L_3 \cosh \gamma L_4 + \sinh \gamma L_4 \cosh \gamma L_3) + \Delta_{52} \cosh \gamma L_3 \cosh \gamma L_4 \quad \text{(A51)}$$

with

$$\Delta_{51} = \sinh \gamma(L_0 - D) \sinh \gamma L_1 \sinh \gamma L_2 + \sinh \gamma(L_0 - D) \cosh \gamma L_1 \cosh \gamma L_2 + \cosh \gamma(L_0 - D) \sinh \gamma L_1 \cosh \gamma L_2 \quad \text{(A52)}$$

$$\Delta_{52} = \cosh \gamma(L_0 - D) \cosh \gamma L_1 \cosh \gamma L_2 + \cosh \gamma(L_0 - D) \sinh \gamma L_1 \sinh \gamma L_2 + \sinh \gamma(L_0 - D) \cosh \gamma L_1 \sinh \gamma L_2. \quad \text{(A53)}$$

For each case we take $F(G, s) = 1$, which gives $f(G, t) = \delta(t)$. Therefore,

$$A(D, s) = \frac{\Delta_5}{\Delta_2}. \quad \text{(A54)}$$

In spite of the extreme complexity of the expression for $A(D, s)$ the expressions $a(D, t)$ for each of the special geometries can be determined analytically in terms of the G-functions. We illustrate with a few samples.

(*a*) $L_i = L$ $(i = 0, 1, 2, 3, 4)$:

$$A(D, s) = \frac{1}{3}\left(\frac{\sinh \gamma(L - D)}{\sinh \gamma L}\right) \coth \gamma L + \frac{2}{9} \frac{\sinh \gamma(L - D)}{\cosh \gamma L} + \frac{1}{9}\left(\frac{\cosh \gamma(L - D)}{\sinh \gamma L}\right) \coth^2 \gamma L + \frac{1}{3} \frac{\cosh \gamma(L - D)}{\sinh \gamma L} \quad \text{(A55)}$$

$$a(D, t) = \tfrac{1}{3} G_{10;s}(L - D, t) * G_{10;c}(L, t) + \tfrac{2}{9} G_{01;s}(L - D, t) + \tfrac{1}{9} G_{10;c}(L - D, t) * G_{10;c}(L, t) * G_{10;c}(L, t) + \tfrac{1}{3} G_{10;c}(L - D, t) \quad \text{(A56)}$$

(*b*) $L_2 \to \infty$, *all other* $L_i = L$:

$$A(D, s) = \frac{\sinh \gamma(L - D)}{4 \sinh \gamma L + 5 \cosh \gamma L}(2 + 2 \coth \gamma L + \coth^2 \gamma L) + \frac{\cosh \gamma(L - D)}{4 \sinh \gamma L + 5 \cosh \gamma L}(2 + \coth \gamma L + \coth^2 \gamma L) \quad \text{(A57)}$$

$$a(D, t) = {}^{58}\!/_{25} G_{45;c}(L - D, t) + {}^{66}\!/_{25} G_{45;s}(L - D, t) + {}^{1}\!/_{25} G_{10;c}(L - D, t) - {}^{4}\!/_{25} G_{10;s}(L - D, t) + {}^{1}\!/_{5} G_{10;c}(L, t) * [G_{10;c}(L - D, t) + 2 G_{10;s}(L - D, t). \quad \text{(A58)}$$

(*c*) $L_3 \to \infty$, $L_4 \to \infty$, *all other* $L_i = L$:

$$A(D, s) = \frac{\sinh \gamma(L - D)}{3(2 \sinh \gamma L + \cosh \gamma L)}[1 + 2 \coth \gamma L + 2 \tanh \gamma L] + \frac{\cosh \gamma(L - D)}{3(2 \sinh \gamma L + \cosh \gamma L)}[1 + \coth \gamma L + \tanh \gamma L] \quad \text{(A59)}$$

$$a(D, t) = \tfrac{1}{3}[2G_{10;s}(L - D, t) + G_{01;s}(L - D, t) - 4G_{21;s}(L - D, t) + G_{10;c}(L - D, t) + \tfrac{1}{2}G_{01;c}(L - D, t) - \tfrac{3}{2}G_{21;c}(L - D, t)]. \quad \text{(A60)}$$

2. Tree With One Primary, Three Secondary Branches (Fig. 6)

Although trifurcation sites are rare our method can, nevertheless, be applied to this type of geometrical pattern. Also, this kind of geometry can approximate the configuration in which there are two bifurcation sites very close together.

A. INPUT ON SECONDARY BRANCH (FIG. 6 *a*)

$$V(0, s) = \frac{Z_c \cosh \gamma(L_1 - D) \cosh \gamma L_2 \cosh \gamma L_3}{\Delta_6} \quad \text{(A61)}$$

where

$$\Delta_6 = \sinh \gamma L_0 \sinh \gamma L_1 \sinh \gamma L_2 \cosh \gamma L_3 + \sinh \gamma L_0 \sinh \gamma L_1 \cosh \gamma L_2 \sinh \gamma L_3 + \sinh \gamma L_0 \cosh \gamma L_1 \sinh \gamma L_2 \sinh \gamma L_3 + \cosh \gamma L_0 \sinh \gamma L_1 \sinh \gamma L_2 \sinh \gamma L_3. \quad \text{(A62)}$$

Choose

$$A(D, s) = \frac{\cosh \gamma(L_1 - D)}{\cosh \gamma L_1} \quad \text{(A63)}$$

$$F(G, s) = \frac{\cosh \gamma L_1 \cosh \gamma L_2 \cosh \gamma L_3}{\Delta_6}. \quad \text{(A64)}$$

(*a*) $L_i = L$ $(i = 0, 1, 2, 3)$: $a(D, t)$ is given by Eq. A8

$$F(G, s) = \frac{1}{4}\frac{\coth^2 \gamma L}{\sinh \gamma L} \quad \text{(A65)}$$

$$f(G, t) = \tfrac{1}{4}G_{10;c}(L, t) * G_{10;c}(L, t) * G_{10;c}(0, t). \quad \text{(A66)}$$

(*b*) $L_1 = 2L$, *all other* $L_i = L$: $a(D, t)$ is given by Eq. A12.

$$F(G, s) = \frac{1}{49}\left[\frac{6}{\sinh \gamma L} + \frac{7}{\coth^2 \gamma L} - 3\left(\frac{1}{\sinh \gamma L + i\sqrt{7}\cosh \gamma L} + \frac{1}{\sinh \gamma L - i\sqrt{7}\cosh \gamma L}\right)\right] \quad \text{(A67)}$$

$$f(G, t) = \tfrac{1}{49}\{6G_{10;c}(0, t) + 7G_{10;c}(L, t) * G_{10;c}(L, t) * G_{10;c}(0, t) - 3[G_{1i\sqrt{7};c}(0, t) + G_{1-i\sqrt{7};c}(0, t)]\}. \quad \text{(A68)}$$

(*c*) $L_2 = 2L$, *all other* $L_i = L$ (*or* $L_3 = 2L$, *all other* $L_i = L$): $a(D, t)$ is given by Eq. A8, $f(G, t)$ by Eq. A68.

(*d*) $L_1 \to \infty$, *all other* $L_i = L$: $a(D, t)$ is given by Eq. A18.

$$F(G, s) = \frac{\coth^2 \gamma L}{\sinh \gamma L + 3 \cosh \gamma L} \tag{A69}$$

$$f(G, t) = \tfrac{1}{3}\, G_{10;c}(0, t) * G_{10;c}(L, t) - \tfrac{1}{9}\, G_{10;c}(0, t) + \tfrac{1}{9}\, G_{13;c}(0, t). \tag{A70}$$

B. INPUT ON PRIMARY BRANCH (FIG. 6 *b*)

$$V(0, s) = \frac{Z_c \Delta_7}{\Delta_6} I_{sy}(s) \tag{A71}$$

where Δ_6 is given by Eq. A62, and

$$\begin{aligned}\Delta_7 = {} & \cosh \gamma(L_0 - D) \cosh \gamma L_1 \cosh \gamma L_2 \sinh \gamma L_3 \\ & + \cosh \gamma(L_0 - D) \cosh \gamma L_1 \sinh \gamma L_2 \cosh \gamma L_3 \\ & + \cosh \gamma(L_0 - D) \sinh \gamma L_1 \cosh \gamma L_2 \cosh \gamma L_3 \\ & + \sinh \gamma(L_0 - D) \cosh \gamma L_1 \cosh \gamma L_2 \cosh \gamma L_3.\end{aligned} \tag{A72}$$

For each case we take $F(G, s) = 1$, and thus $f(G, t) = \delta(t)$.

$$A(D, s) = \frac{\Delta_7}{\Delta_6} \tag{A73}$$

(*a*) $L_i = L$ $(i = 0, 1, 2, 3)$:

$$A(D, s) = \frac{3}{4}\left[\frac{\cosh \gamma(L - D)}{\sinh \gamma L}\right] \coth \gamma L + \frac{1}{4}\left[\frac{\sinh \gamma(L - D)}{\sinh \gamma L}\right] \coth^2 \gamma L \tag{A74}$$

$$\begin{aligned}a(D, t) = {} & \tfrac{3}{4}\, G_{10;c}(L, t) * G_{10;c}(L - D, t) \\ & + \tfrac{1}{4}\, G_{10;c}(L, t) * G_{10;c}(L, t) * G_{10;s}(L - D, t)\end{aligned} \tag{A75}$$

(*b*) $L_1 \to \infty$, *all other* $L_i = L$ *(or* $L_2 \to \infty$ *or* $L_3 \to \infty$, *all other* $L_i = L$*)*:

$$\begin{aligned}A(D, s) = \coth \gamma L \Bigg[& \frac{\cosh \gamma(L - D) + \tfrac{1}{3} \sinh \gamma(L - D)}{\sinh \gamma L + 3 \cosh \gamma L} \\ & + \frac{\cosh \gamma(L - D) + \sinh \gamma(L - D)}{3 \sinh \gamma L}\Bigg]\end{aligned} \tag{A76}$$

$$\begin{aligned}a(D, t) = {} & \tfrac{1}{3}\, [G_{10;c}(L - D, t) - G_{13;c}(L - D, t)] \\ & + \tfrac{1}{9}\, [G_{10;s}(L - D, t) - G_{13;s}(L - D, t)] \\ & + \tfrac{1}{3}\, G_{10;c}(L, t) * [G_{10;c}(L - D, t) + G_{10;s}(L - D, t)].\end{aligned} \tag{A77}$$

(*c*) $L_0 = L_1 = L$, $L_2 \to \infty$, $L_3 \to \infty$ *(or* $L_0 = L_i = L$, $L_j, L_k \to \infty$*)*:

$$\begin{aligned}A(D, s) = {} & \frac{\cosh \gamma(L - D)}{\sinh \gamma L} + \frac{\sinh \gamma(L - D)}{2 \sinh \gamma L} \\ & - \frac{\cosh \gamma(L - D)}{2(\sinh \gamma L + \cosh \gamma L)} - \frac{\sinh \gamma(L - D)}{2(\sinh \gamma L + \cosh \gamma L)}\end{aligned} \tag{A78}$$

$$a(D, t) = G_{10;c}(L - D, t) + \tfrac{1}{2} G_{10;s}(L - D, t) - \tfrac{1}{2} G_{11;c}(L - D, t) - \tfrac{1}{2} G_{11;s}(L - D, t). \quad \text{(A79)}$$

Many other examples could be given. For each primitive integral geometry the expressions for $a(D, t)$ and $f(G, t)$ can always be written in terms of the G-functions.

APPENDIX B

To show the simplicity that results when the G-function notation is used, I shall write some of the expressions obtained earlier in this paper in the more traditional way, which involves the use of theta and modified theta functions.

Consider the geometry of Fig. 4 *a*. We found for the case where all three branches were of equal length that

$$a(D, t) = G_{01;c}(L - D, t) \quad \text{(B1)}$$

$$f(G, t) = \tfrac{1}{3} G_{10;c}(0, t). \quad \text{(B2)}$$

The equivalent expressions, using the notation of Oberhettinger and Badii (1973), are

$$a(D, t) = -\frac{\lambda^2}{L\tau} e^{-t/\tau} \frac{\partial \theta_1\left(\frac{L - D}{2L} \middle| \frac{\lambda^2 t}{L^2 \tau}\right)}{\partial(\mathrm{L} - \mathrm{D})} \quad \text{(B3)}$$

$$f(G, t) = \frac{\lambda}{3L\sqrt{\tau}} e^{-t/\tau} \left[\frac{\partial \hat{\theta}_4\left(\frac{\nu\lambda}{2\sqrt{\tau}L} \middle| \frac{\lambda^2 t}{L^2 \tau}\right)}{\partial \nu}\right]_{\nu=0} \quad \text{(B4)}$$

θ_1 is one of the theta functions; $\hat{\theta}_4$ is one of the modified theta functions. They are defined in Oberhettinger and Badii (1973).

A second example uses the geometry of Fig. 4 *b* (input on the primary branch). We found for equal lengths

$$a(D, t) = \tfrac{2}{3} G_{01;s}(L - D, t) + \tfrac{1}{3} G_{10;c}(L - D, t). \quad \text{(B5)}$$

Use of the theta function notation gives us instead

$$a(D, t) = \frac{\lambda^2 e^{-t/\tau}}{3L\tau}\left[2\frac{\partial \hat{\theta}_1\left(\frac{L - D}{2L} \middle| \frac{\lambda^2 t}{L^2 \tau}\right)}{\partial(L - D)} - \frac{\partial \hat{\theta}_4\left(\frac{L - D}{2L} \middle| \frac{\lambda^2 t}{L^2 \tau}\right)}{\partial(L - D)}\right]. \quad \text{(B6)}$$

The G-function formalism provides a much less cumbersome notation, especially for the more complicated expressions. Indeed, if we take the case of $L_0 = L_1$ and $L_2 \to \infty$ for the geometry of Fig. 4 *b*, the expression for $a(D, t)$ cannot even be expressed in the theta function form in any simple way. This situation holds for most of the geometries we considered in this paper.

I wish to thank Dr. G. Gross for many useful discussions. An anonymous referee provided a number of useful suggestions. I also wish to thank Beth Romines for typing the manuscript and Terry Zirn for aid in preparing the illustrations.

This research was supported in part by institutional research grants from Texas Woman's University.

Received for publication 3 March 1980 and in revised form 14 February 1981.

REFERENCES

Barrett, J. N., and W. E. Crill. 1974*a*. Specific membrane properties of cat motoneurones. *J. Physiol. (Lond.)*. 239:301–324.

Barrett, J. N., and W. E. Crill. 1974*b*. The influence of dendritic location and membrane properties on the effectiveness of synapses on cat motoneurones. *J. Physiol. (Lond.)*. 239:325–345.

Buell, S. J., and P. D. Coleman. 1979. Dendritic growth in the aged human brain and failure of growth in senile dementia. *Science (Wash., D.C.)*. 206:854–856.

Butz, E. G., and J. D. Cowan. 1974. Transient potentials in dendritic systems of arbitrary geometry. *Biophys. J.* 14:661–689.

Christensen, B. N., and F. F. Ebner. 1978. The synaptic architecture of neurons in opossum somatic sensory-motor cortex: a combined anatomical and physiological study. *J. Neurocytol.* 7:39–60.

Christensen, B. N., and W. P. Teubl. 1979. Estimates of cable parameters in lamprey spinal cord neurones. *J. Physiol. (Lond.)*. 297:299–318.

Churchill, R. V. 1958. Operational Mathematics. McGraw-Hill, New York.

Davis, P. J., and P. Rabinowitz. 1975. Methods of Numerical Integration. Academic Press, Inc., New York.

Davis, T. L., and P. Sterling. 1979. Microcircuitry of cat visual cortex: classification of neurons in layer IV of area 17, and identification of patterns of lateral geniculate input. *J. Comp. Neurology*. 188:599–628.

Diamond, J., E. G. Gray, and G. M. Yasargil. 1970. The function of the dendritic spine: an hypothesis. *In* Excitatory Synaptic Mechanisms. P. Andersen and J. K. S. Jansen, editors. Universitetsforlaget, Oslo.

Fiala, B. A., J. N. Joyce, and W. T. Greenough. 1978. Environmental complexity modulates growth of granule cell dendrites in developing but not adult hippocampus of rats. *Exp. Neurol.* 59:372–383.

Gilbert, C. D., and T. N. Wiesel. 1979. Morphology and intracortical projections of functionally characterised neurones in the cat visual cortex. *Nature (Lond.)*. 280:120–125.

Glasser, S. 1977. Computer Reconstruction and Passive Modeling of Identified Nerve Cells in the Lobster Stomatogastric Ganglion. Ph.D. Thesis. University of California, San Diego, California.

Greenough, W. T., J. M. Juraska, and F. R. Volkmar. 1979. Maze training effects on dendritic branching in occipital cortex of adult rats. *Beh. and Neural Biol.* 26:287–297.

Greenough, W. T., and F. R. Volkmar. 1973. Pattern of dendritic branching in occipital cortex of rats reared in complex environments. *Exp. Neurol.* 41:371–378.

Gutnick, M. J., and D. A. Prince. 1981. Dye coupling and possible electrotonic coupling in the guinea pig neocortical slice. *Science (Wash., D.C.)*. 211:67–70.

Higgins, M. L., M. N. Smith, and G. W. Gross. 1980. Selective cell destruction and precise neurite transection in neuroblastoma cultures with pulsed ultraviolet laser microbeam irradiation: An analysis of mechanisms and transection reliability with light and scanning electron microscopy. *J. Neurosci. Methods*. 3:83–99.

Hillman, D. E. 1979. Neuronal shape parameters and substructures as a basis of neuronal form. *In* The Neurosciences: Fourth Study Program. F. O. Schmitt and F. G. Worder, editors. MIT Press, Cambridge, Mass.

Horwitz, B. 1981. Neuronal plasticity: how changes in dendritic architecture can affect the spread of postsynaptic potentials. *Brain Res.* In press.

Jack, J. J. B., D. Noble, and R. W. Tsien. 1975. Electric Current Flow in Excitable Cells. Oxford University Press, Oxford.

Jack, J. J. B., and S. J. Redman. 1971*a*. The propagation of transient potentials in some linear cable structures. *J. Physiol. (Lond.)*. 215:283–320.

Jack, J. J. B., and S. J. Redman. 1971*b*. An electrical description of the motoneuron, and its application to the analysis of synaptic potentials. *J. Physiol. (Lond.)*. 215:321–352.

Lindsay, R. D. (editor). 1977. Computer Analysis of Neuronal Structures. Plenum Press, New York.

Llinas, R., and C. Nicholson. 1971. Electrophysiological properties of dendrites and somata in alligator Purkinje cell. *J. Neurophysiol.* 34:532–551.

Lux, H. D., P. Schubert, and G. W. Kreutzberg. 1970. Direct matching of morphological and electrophysiological data in cat spinal motoneurones. *In* Excitatory Synaptic Mechanisms. P. Andersen and J. K. S. Jansen, editors. Universitetsforlaget, Oslo.

Mehraein, P., M. Yamada, and E. Tarnowska-Dziduszko. 1975. Quantitative study on dendrites and dendritic spines in Alzheimer's disease and senile dementia. *In* Advances in Neurology, Vol. 12. G. W. Kreutzberg, editor. Raven Press, New York.

Oberhettinger, F., and L. Badii. 1973. Tables of Laplace Transforms. Springer-Verlag, New York.

Perkel, D. H., and B. Mulloney. 1978. Electrotonic properties of neurons: steady-state compartmental model. *J. Neurophysiol.* 41:621–639.

Pinching, A. J., and T. P. S. Powell. 1971. The neuropil of the glomeruli of the olfactory bulb. *J. Cell Sci.* 9:347–377.

Purpura, D. P. 1974. Dendritic spine "dysgenesis" and mental retardation. *Science (Wash., D.C.).* 186:1126–1128.

Rakic, P. (editor). 1976. Local Circuit Neurons. MIT Press, Cambridge, Mass.

Rall, W. 1959. Branching dendritic trees and motoneuron membrane resistivity. *Exp. Neurol.* 1:491–527.

Rall, W. 1960. Membrane potential transients and membrane time constant of motoneurons. *Exp. Neurol.* 2:503–532.

Rall, W. 1962*a*. Theory of physiological properties of dendrites. *Ann. N.Y. Acad. Sci.* 96:1071–1092.

Rall, W. 1962*b*. Electrophysiology of a dendritic neuron model. *Biophys. J.* 2:145–167.

Rall, W. 1964. Theoretical significance of dendritic trees for neuronal input-output relations. *In* Neural Theory and Modeling. R. F. Reiss, editor. Stanford University Press, Stanford, California.

Rall, W. 1967. Distinguishing theoretical synaptic potentials computed for different soma-dendritic distributions of synaptic input. *J. Neurophysiol.* 30:1138–1168.

Rall, W. 1969. Time constants and electrotonic length of membrane cylinders and neurons. *Biophys. J.* 9:1483–1508.

Rall, W. 1970. Cable properties of dendrites and effects of synaptic location. *In* Excitatory Synaptic Mechanisms. P. Andersen and J. K. S. Jansen, editors. Universitetsforlaget, Oslo.

Rall, W. 1977. Core conductor theory and cable properties of neurons. *In* Handbook of Physiology (*Sect. 1*) The Nervous System. I. Cellular Biology of Neurons. E. R. Kandel, editor. *Am. Physiol. Soc.*, Bethesda, Md. 39–97

Rall, W., R. E. Burke, T. G. Smith, and K. Frank. 1967. Dendritic location of synapses and possible mechanisms for the monosynaptic EPSP in motoneurons. *J. Neurophysiol.* 30:1169–1193.

Rall, W., and J. Rinzel. 1973. Branch input resistance and steady attenuation for input to one branch of a dendritic neuron model. *Biophys. J.* 13:648–688.

Rall, W., G. M. Shepherd, T. S. Reese, and M. W. Brightman. 1966. Dendro-dendritic synaptic pathway for inhibition in the olfactory bulb. *Exp. Neurol.* 14:44–56.

Redman, S. J. 1973. The attenuation of passively propagating dendritic potentials in a motoneurone cable model. *J. Physiol. (Lond.).* 234:637–664.

Redman, S. J. 1976. A quantitative approach to integrative function of dendrites. *In* International Review of Physiology, Vol. 10, Neurophysiology II. R. Porter, editor. University Park Press, Baltimore, Md.

Rieske, E., G. W. Gross, and G. W. Kreutzberg. 1977. Laser in der experimentellen Zellforschung. *Laser Electro-Optik.* 2:44–45.

Rieske, E., and G. W. Kreutzberg. 1978. Neurite regeneration after cell surgery with laser microbeam irradiation. *Brain Res.* 148:478–483.

Rinzel, J., and W. Rall. 1974. Transient response in a dendritic neuron model for current injected at one branch. *Biophys. J.* 14:759–790.

Schmitt, F. O., P. Dev, and B. H. Smith. 1976. Electrotonic processing of information by brain cells. *Science (Wash., D.C.).* 193:114–120.

Schmitt, F. O., and F. G. Worden (editors). 1979. The Neurosciences: Fourth Study Program. MIT Press, Cambridge, Mass.

Shepherd, G. M. 1979. The Synaptic Organization of the Brain. Oxford University Press, Oxford, England.

Stretton, A. O. W., and E. A. Kravitz. 1968. Neuronal geometry: determination with a technique of intracellular dye injection. *Science (Wash., D.C.).* 162:132–134.

Van Essen, D., and J. Kelley. 1973. Morphological identification of simple, complex and hypercomplex cells in the visual cortex of the cat. *In* Intracellular Staining in Neurobiology. S. B. Kater and C. Nicholson, editors. Springer-Verlag, New York.

White, E. L. 1972. Synaptic organization in the olfactory glomerulus of the mouse. *Brain Res.* 37:69–80.

Widder, D. V. 1975. The Heat Equation. Academic Press, Inc., New York.